AD-A070 309 RHODE ISLAND UNIV KINGSTON DEPT OF OCEAN ENGINEERING F/G 11/6
HYDROGEN PERMEATION IN IRON AT LOW TEMPERATURES.(U)
MAR 79 M SURKEIN, R H HEIDERSBACH DAAG29-76-G-0311
UNCLASSIFIED TR-1 ARO-14057.3-MS NL

1 OF 2
AD A070309

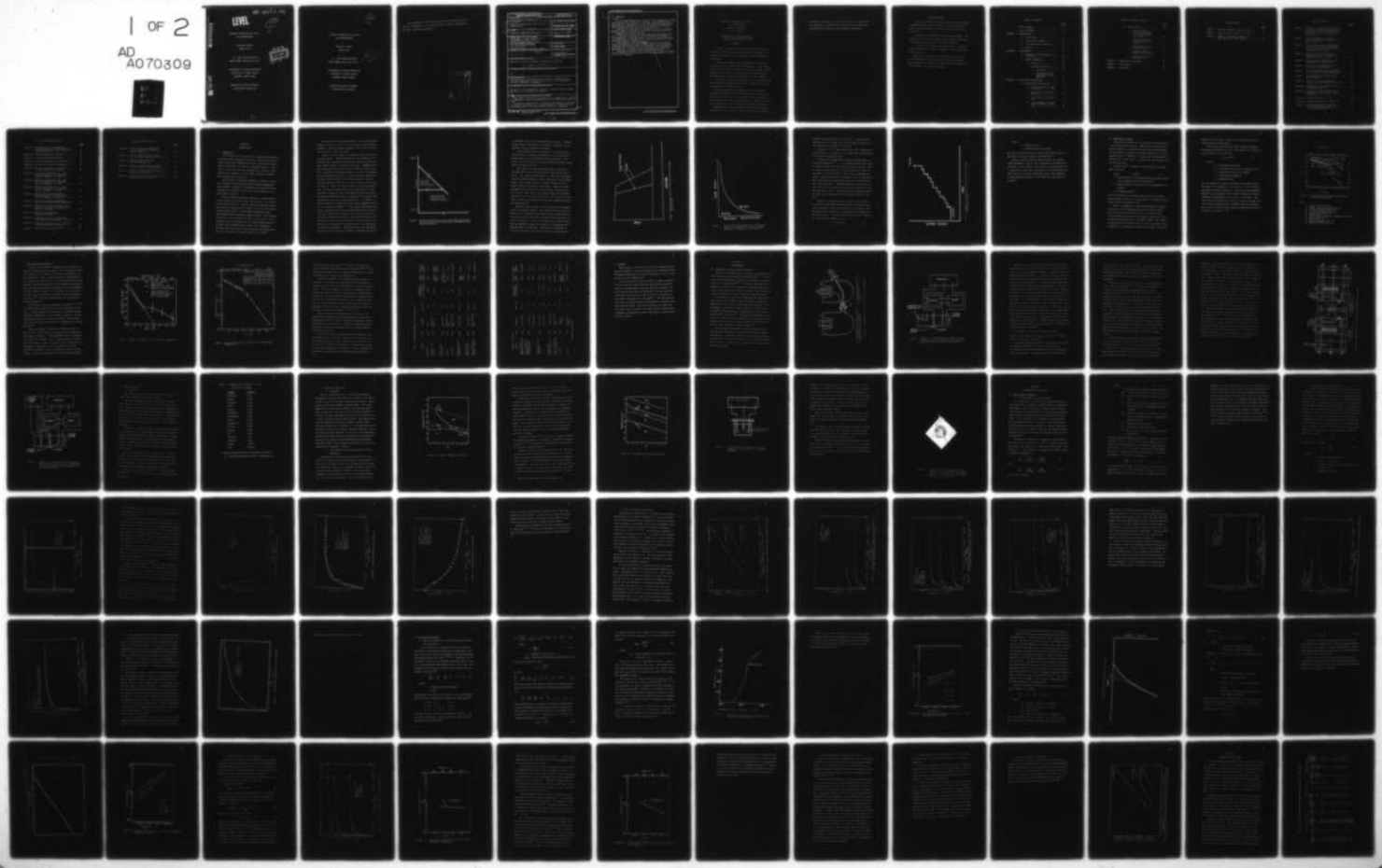

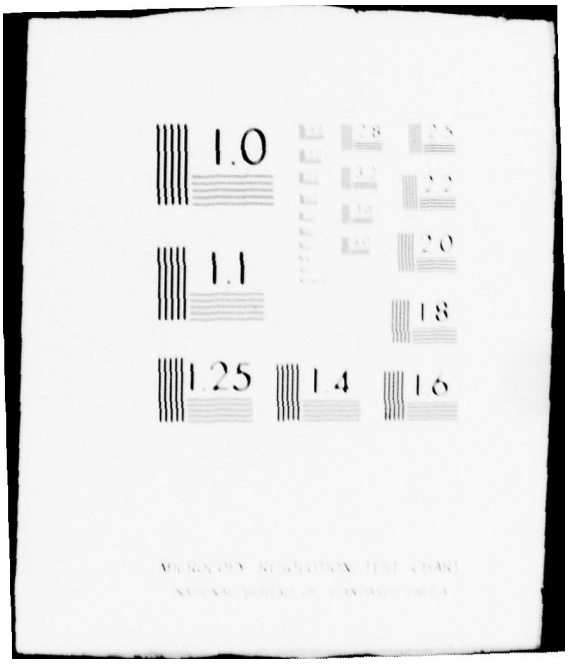
1.0
1.1
1.25
1.4
1.6
2.0
1.8

LEVEL II

12

HYDROGEN PERMEATION IN IRON AT LOW TEMPERATURES

TECHNICAL REPORT

MARCH 1979

U.S. ARMY RESEARCH OFFICE

GRANT NUMBER DAAG 29-76-G-0311

DEPARTMENT OF OCEAN ENGINEERING

UNIVERSITY OF RHODE ISLAND

KINGSTON, RHODE ISLAND

APPROVED FOR PUBLIC RELEASE:

DISTRIBUTION UNLIMITED

(12)

HYDROGEN PERMEATION IN IRON AT LOW TEMPERATURES

TECHNICAL REPORT

MARCH 1979

U.S. ARMY RESEARCH OFFICE

GRANT NUMBER DAAG 29-76-G-0311

DEPARTMENT OF OCEAN ENGINEERING

UNIVERSITY OF RHODE ISLAND

KINGSTON, RHODE ISLAND

APPROVED FOR PUBLIC RELEASE:

DISTRIBUTION UNLIMITED

The findings in this report are not to be construed as an official Department of the Army position, unless so designated by other authorized documents.

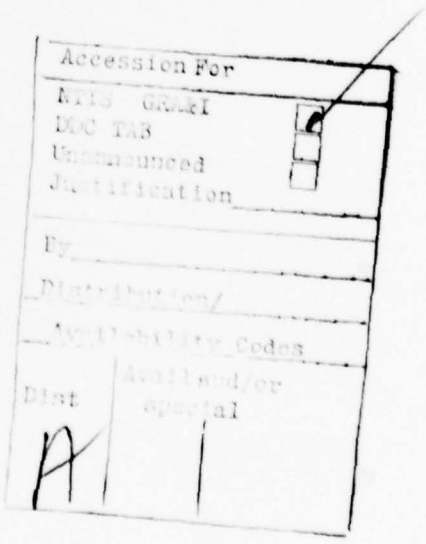

SECURITY CLASSIFICATION OF THIS PAGE (When Data Entered)

REPORT DOCUMENTATION PAGE

READ INSTRUCTIONS BEFORE COMPLETING FORM

1. REPORT NUMBER: Interim Technical Report #I
2. GOVT ACCESSION NO.
3. RECIPIENT'S CATALOG NUMBER

4. TITLE (and Subtitle): Hydrogen Permeation in Iron at Low Temperatures.
5. TYPE OF REPORT & PERIOD COVERED: Master's Thesis
6. PERFORMING ORG. REPORT NUMBER

7. AUTHOR(s): M. Surkein and R. Heidersbach, Jr.
8. CONTRACT OR GRANT NUMBER(s): DAAG 29-76-G-0311

9. PERFORMING ORGANIZATION NAME AND ADDRESS
Department of Ocean Engineering,
University of Rhode Island
Kingston, Rhode Island 02881

10. PROGRAM ELEMENT, PROJECT, TASK AREA & WORK UNIT NUMBERS

11. CONTROLLING OFFICE NAME AND ADDRESS
U.S. Army Research Office
P.O. Box 12211
Research Triangle Park, NC 27709

12. REPORT DATE: May 77
13. NUMBER OF PAGES: 105 p.

14. MONITORING AGENCY NAME & ADDRESS (if different from Controlling Office): TR-1

15. SECURITY CLASS. (of this report): Unclassified
15a. DECLASSIFICATION/DOWNGRADING SCHEDULE: N/A

16. DISTRIBUTION STATEMENT (of this Report)
Approved for Public Release; Distribution Unlimited
ARO 14457.3-MS

17. DISTRIBUTION STATEMENT (of the abstract entered in Block 20, if different from Report)
N/A

18. SUPPLEMENTARY NOTES
The findings of this report are not to be construed as an official Department of the Army position, unless designated by other authorized documents.

19. KEY WORDS (Continue on reverse side if necessary and identify by block number)
Corrosion, electrochemistry, hydrogen, hydrogen embrittlement, metals, iron, diffusion, palladium

20. ABSTRACT (Continue on reverse side if necessary and identify by block number)
This report contains the manuscript of a thesis by M. Surkein, MS candidate in Ocean Engineering at the University of Rhode Island.

A study of concentration, thickness and temperature effects on hydrogen permeation in iron was conducted. This study was performed using a gas phase hydrogen charging technique.

DD FORM 1 JAN 73 1473 EDITION OF 1 NOV 65 IS OBSOLETE
S/N 0102-LF-014-6601

SECURITY CLASSIFICATION OF THIS PAGE (When Data Entered)

407 892 LB

20. ABSTRACT

Initial experiments were to observe the permeation fluxes to see if steady states were reached. Once steady states were reached, the effects of electroplated palladium surface coatings were measured by varying the palladium thickness and by using uncoated inlet or exit surfaces.

Variations in specimen thickness and in inlet hydrogen pressure demonstrated that the overall transport rate was not dependent on surface effects.

Comparisons between gas phase charging experiments led to the tentative conclusion that differences in shapes of the permeation curves obtained by the two techniques are due to differences in hydrogen flux levels produced by the two different charging techniques.

Experiments in which membrane thickness and hydrogen charging pressure were kept constant while varying temperatures were performed to observe the effects of temperature on permeation. Arrhenius plots were drawn and activation energies were calculated using standard techniques.

Effective (apparent diffusivities) and lattice diffusivities of hydrogen in Ferrovac-E iron were measured at 5×10^{-7} to 53×10^{-7} cm^2/sec.

Hydrogen Permeation in Iron at Low Temperatures

Michael B. Surkein

M. S. Thesis

Department of Ocean Engineering
University of Rhode Island
Kingston, Rhode Island 02881

ABSTRACT

A study of concentration, thickness and temperature effects on hydrogen permeation in iron was conducted. This study was performed using a gas phase hydrogen charging technique.

Initial experiments were to observe the permeation fluxes to see if steady states were reached. Once steady states were reached, the effects of electroplated palladium surface coatings were measured by varying the palladium thickness and by using uncoated inlet or exit surfaces.

Variations in specimen thickness and in inlet hydrogen pressure demonstrated that the overall transport rate was not dependent on surface effects.

Comparisons between gas phase and electrochemical charging experiments led to the tentative conclusion that differences in shapes of the permeation curves obtained by the two techniques are due to differences in hydrogen flux levels produced by the two different charging techniques.

Experiments in which membrane thickness and hydrogen charging pressure were kept constant while varying tempera-

tures were performed to observe the effects of temperature on permeation. Arrhenius plots were drawn and activation energies were calculated using standard techniques.

ACKNOWLEDGEMENTS

I wish to express my sincere appreciation to Dr. Robert H. Heidersbach Jr. whose guidance, criticism and overall support was instrumental in the successful completion of this work.

I also wish to thank my fellow graduate students and friends for their moral support, encouragement and friendliness during my two year stay in Rhode Island.

I also with to express my appreciation to the United States Army Research Office - Durham, for the sponsorship of this project.

Most of all I would like to express lifelong heartfelt gratitude to my family, Carol, Stanley and Elana, whose constant love, devotion and encouragement made possible my pursuit of higher education.

TABLE OF CONTENTS

TABLE OF CONTENTS (cont'd)

LIST OF TABLES

LIST OF FIGURES

LIST OF FIGURES (cont'd)

LIST OF FIGURES (cont'd)

CHAPTER 1

INTRODUCTION

A. Background

The recognition of hydrogen as a deleterious solute in steels and other materials has been a subject of broad interest since this phenomenon was first reported by Claire Deville and Troost[1] in the mid nineteenth century. Since then, it has been seen that hydrogen has a role in inducing brittle failure in a wide range of metallic systems, both ferrous and non ferrous.

The presence of absorbed hydrogen in metals is of special interest to the petroleum and aerospace industries. The aerospace industry is continuously designing aircraft, missiles and spacecraft using high strength metals to reduce weight and cost.

Failure caused by absorbed hydrogen in parts such as wings, fasteners and fuel tanks can be costly. If failure occurs during service, injury or death may possibly result. This problem became quite noticeable in 1965 in the United States space program. Large storage vessels for high purity-high pressure hydrogen began failing[2]. Six failures occurred in five tanks made of low strength steel, not previously known to be susceptible to hydrogen embrittlement[2]. In 1968, high strength nickel alloys used in hydrogen storage vessels for mariner space vehicles were found subject to the same form of embrittlement as in 1965[2].

Failures due to absorbed hydrogen in the petroleum industry are usually not as costly as those in the aerospace industry. The most common problem is the failure of structural steels in sour oil wells[3].

There are three common environmental ways for hydrogen to enter metals[4]. Metal exposures to high temperature or high pressure hydrogen-containing environments are the two most common sources of hydrogen in metals. Combinations of high temperature-high pressure environments are also common. Electrolytic hydrogen deposition is the third common source of hydrogen in metals. The electrolytic method is the most potent process to introduce hydrogen, since it sustains enormous fugacities of atomic hydrogen at the metal surface[4]. There are many sources of electrolytic hydrogen. In the petroleum industry, the usual source is the corrosion reaction of steel with aqueous hydrogen sulfide solutions, encountered either in production of crude oil and natural gas or in oil refining operations. In Figure 1, a potential-pH plot, some processes by which hydrogen can enter into metals are shown[4]. In the region below water stability, hydrogen can be evolved spontaneously in corrosion, pickling, and battery (galvanic cell) operations without external current being applied. Below the stability of the m-ion, where there is application of external current, hydrogen can be produced in electroplating, electrowinning, and cathodic protection. Hydrogen can be electrolytically introduced into a particular metallic component during any

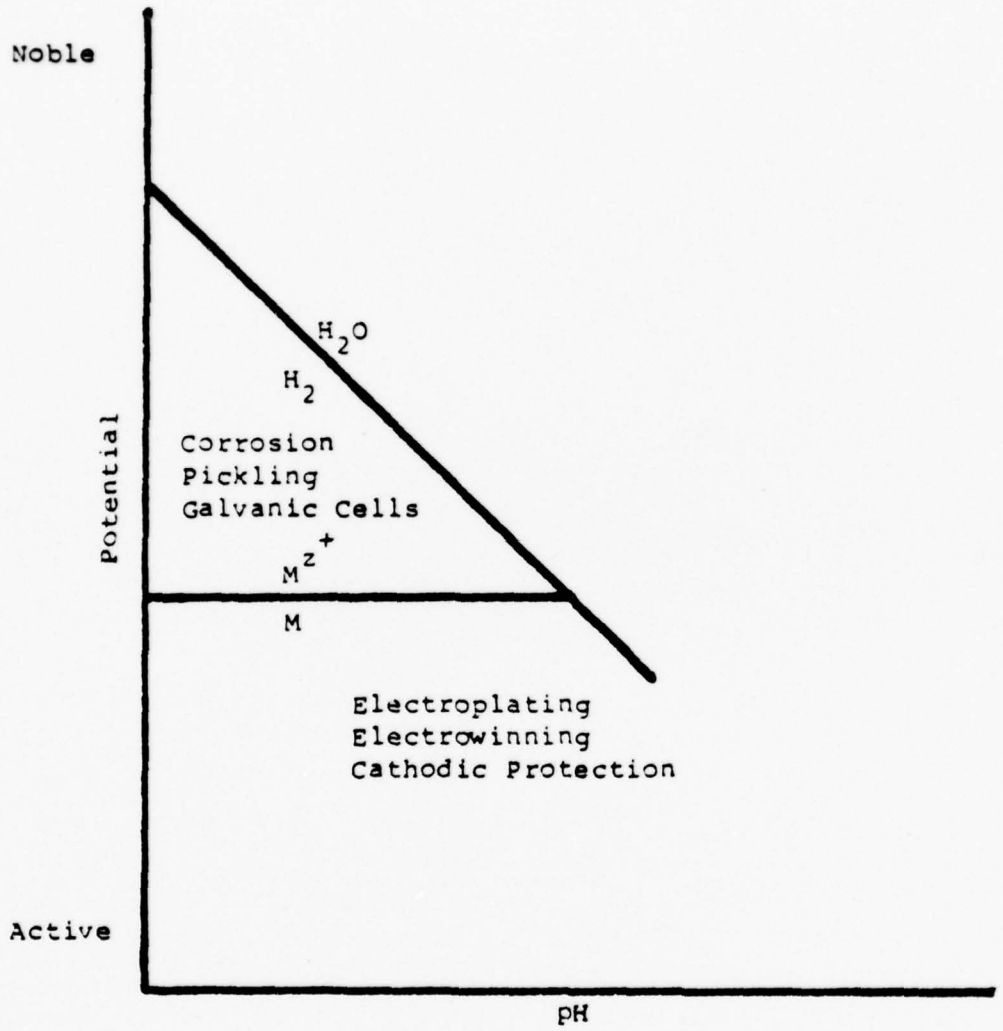

FIGURE 1: Potential-pH Diagram of an Active Metal Water System Showing the Regions Where Various Electrochemical Processes Can Cause Hydrogen Production[4]

of the many steps in its preparation or service. Other hydrogen sources include de-icing fluids, chemicals for degreasing, paint stripping and etching.

High strength steels are subject to delayed brittle failure under a steadily applied relatively low external stress when they are contaminated with hydrogen[5]. The steels lose their ductility by the formation of microcracks within the metal lattice.

The kinetics of hydrogen embrittlement can be described with the aid of a load versus time diagram (Figure 2). At certain stress levels a crack will form after a period called incubation time. This crack will propagate slowly, and in most cases the stress intensity at the crack tip will rise as the crack grows. When the stress intensity factor reaches a critical value, rapid failure will occur[2]. When the initial stress level is increased incubation time and crack propagation time tend to decrease until a stress level where failure occurs immediately upon load application[2].

When the initial stress level stays below a threshold value, no failure occurs[2]. The threshold stress value appears to be a function of hydrogen content of the material, and will be higher the lower the hydrogen concentration, as shown in Figure 3[5]. This is the reason why a baking treatment is applied to steel parts that are contaminated with hydrogen due to processing. This baking is expected to drive out quantities of hydrogen, therefore reducing the

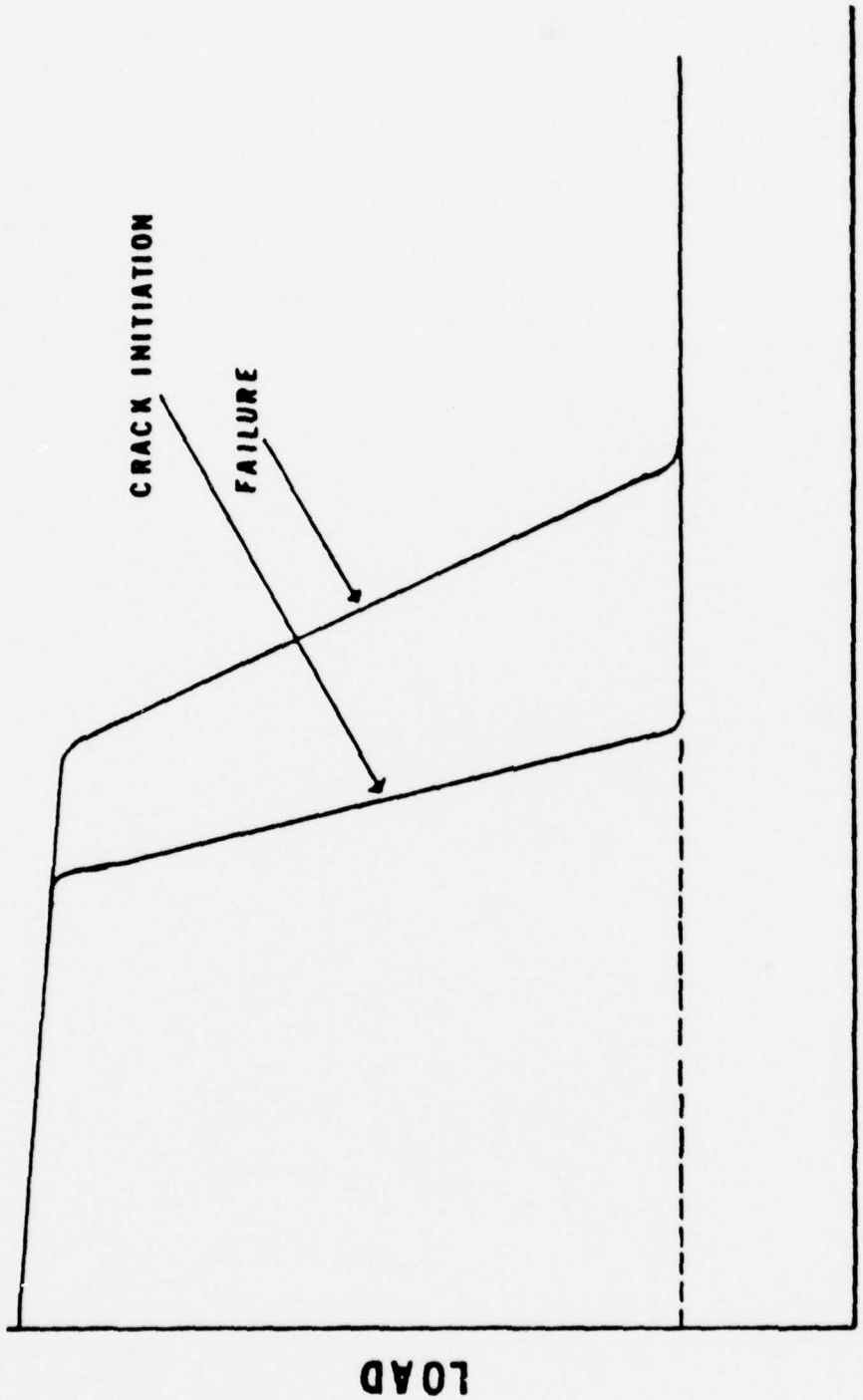

FIGURE 2: The Characteristic Diagram of Load versus Time for Hydrogen Induced Failure[2]

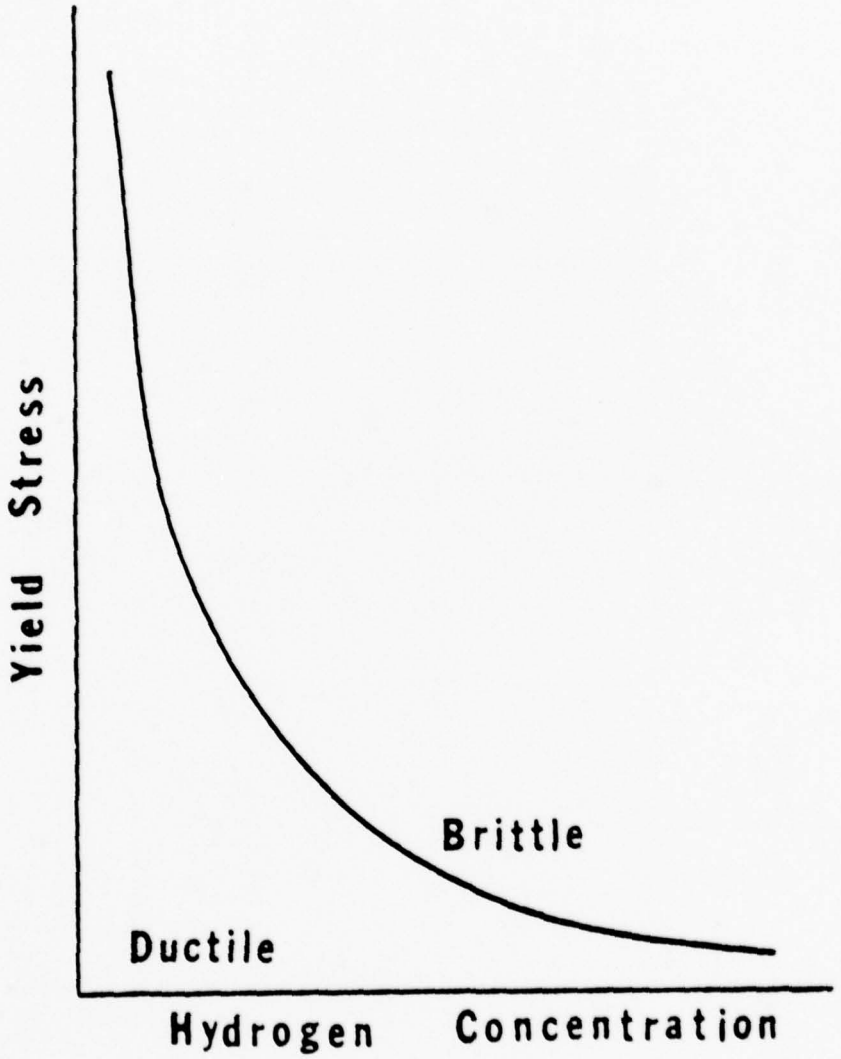

FIGURE 3: Yield Stress Versus Hydrogen Concentration Showing the Dependence of the Stress for Fracture on the Hydrogen Concentration[5]

hydrogen concentration to a safe level[2]. The outcome of this process is to raise the critical stress level above the stress level expected in service[2].

Troiano, et. al.[6] have shown that crack propagation is discontinuous. In Figure 4 it is shown that crack propagation occurs in discrete steps.

It has been proposed that hydrogen embrittlement is diffusion dependent[7-11]. It is argued that hydrogen tends to diffuse towards the most highly stressed regions. When a critical combination of stress and hydrogen content is attained, a crack initiates[2]. The crack is arrested because, although the stress intensity at its tip may be high, the local hydrogen concentration will be too low for further crack extension. Hydrogen diffusion will now occur until the crack tip condition is critical again and a second burst will occur[2]. Repetition of this process continues until the discontinuous crack growth results in failure[2].

Zapfee[12] proposed the planar pressure theory which says that hydrogen embrittlement results from the precipation of hydrogen gas at defects such as inclusions. The pressure causes expansion of microcracks and voids due to the gas pressure[7]. Borelius and Lindblom (1927)[13] reported the internal gas pressure to be:

$$P = 17{,}000\ i \qquad (1)$$

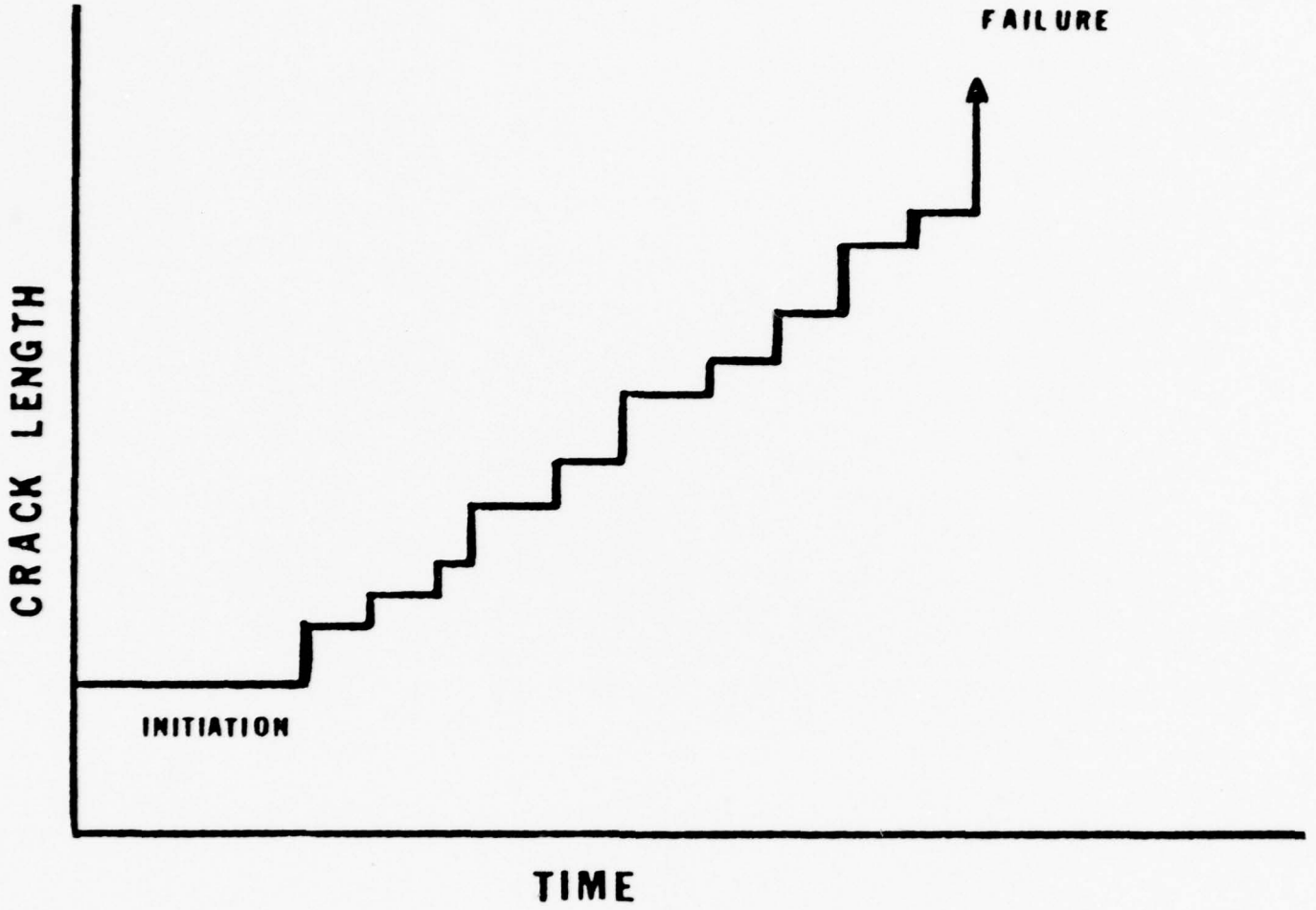

FIGURE 4: Stepwise Crack Growth Due to Hydrogen Diffusion, Subsequent Embrittlement and Failure[6]

where:

P = pressure in atm

i = current density in amp/cm^2

The planar pressure theory was later modified by many researchers, including Tetelman and Robertson[14].

As one can see, hydrogen embrittlement is a complicated phenomenon, and its exact explanation has been quite uncertain. But no matter how uncertain the explanation, it is important to note that hydrogen has a maximum embrittlement effect in the same temperature range where anomalies in both hydrogen solubility and diffusivity have been reported[15].

B. Experimental System

Much work has been done on solubility and diffusivity in the hydrogen-iron system. These results are often not easily compared or generalized because of the differences in experimental techniques, material composition, and processing history. Therefore, a clear and concise characterization over a wide range of temperatures and pressures has not been obtained.

Sieverts Law[16], expresses the solubility of diatomic gases in metals:

where: $$C = SP^{1/2} \qquad (2)$$

C = concentration of dissolved hydrogen in equilibrium with gaseous hydrogen at pressure P

S = proportionality constant which is temperature dependent

P = hydrogen pressure

The $P^{1/2}$ dependence of hydrogen concentration indicates that hydrogen enters iron in the atomic or dissociated form rather than the molecular form[17].

There is substantial evidence that hydrogen in solid solution in iron occupies interstitial lattice sites[18]. This is suggested by the small size of hydrogen atom, 1.06^{o}A diameter, and by the large equilibrium partial molal volume of hydrogen in iron, 2.0 cm^3/g atom[19]. At 1.06^{o}A the hydrogen atom is much smaller than an iron atom, 2.52^{o}A diameter, it is therefore unlikely to have such a large and

positive partial molal volume if the hydrogen existed at substitutional lattice sites.

The previous information tends to suggest hydrogen diffuses interstitally in iron. The equation for interstitial diffusion is as follows[13]:

$$D = Do\ e^{-Q/RT} \qquad (3)$$

where:

D = diffusion coefficient

Do = pre-exponential term or frequency factor

Q = activation energy of diffusion

R = universal gas constant

T = temperature K^{o}.

The pre-exponential term Do, has been calculated by Wert and Zener[20] for hydrogen in iron to be 1.6×10^{-3} cm^2/sec, assuming interstital diffusion. Using the same assumption, McNeil[21] has calculated the activation energy for lattice diffusion of hydrogen in iron to be 1.3 Kcal/mole. The theoretical pre-exponental term, Do, of Wert and Zener and the activation energy value of McNeil compare reasonably well with the range of high temperature experimental values as shown in Figure 5[15, 28].

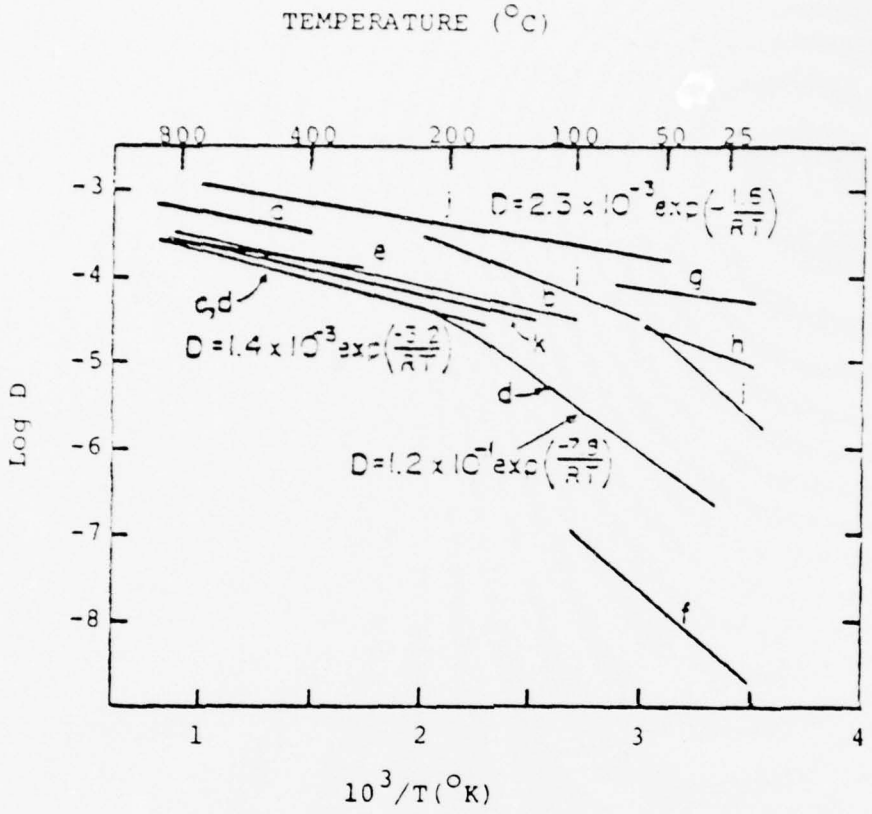

Figure 5: Diffusivity of Hydrogen in Iron Versus Inverse Temperature[15]

Note:

a. Geller and Sun (Ref.22)
b. Sykes, Burton and Gregg (Ref. 23)
c. Stross and Tompkins (Ref. 24)
d. Hill and Johnson (Ref. 17)
e. Heumann and Primas (Ref. 25)
f. Barrer (Ref. 26)
g. Beck, Rockris, McBreen, and Nanis (Ref. 27)
h. Kumnick (Ref. 18)
i. Quick (Ref. 28)
j. Nelson and Stein (Ref. 29)
k. Bryan and Dodge (Ref. 30)

C. Low Temperature Anomalies

In spite of the general agreement of the physical aspects of the hydrogen-iron system, conflicting data on both the diffusivity and solubility have been reported in the low temperature ranges. Hill and Johnson[31] reported positive deviations from Sievert's law and showed that low temperature measured solubilities were substantially greater than values predicted by extrapolation of the high temperature data shown in Figure 6. The dashed line in Figure 6 is taken from the equation of solubility calculated by Geller and Sun[22]. The same deviation was also observed by Chang and Bennett[32].

The results of other experimental studies[17, 18, 22-30] on diffusivity of hydrogen in iron are summarized in Figure 5, in which apparent diffusivity D is plotted against reciprocal temperature. As is shown in Figure 5, as temperature decreases the scatter increases. This scatter cannot be attributed to variation in composition of tested material[18].

Hill and Johnson[31] observed an anomalous break at about 200°C in the diffusivity versus inverse temperature plot shown in Figure 7. This phenomenon was not observed by Stross and Tompkins[24] using a method similar to that of Hill and Johnson. Bryan and Dodge[30] using a different experimental technique also did not observe the break. Quick[28] did observe a break at 70°C while using a vacuum method. Also the low temperature diffusivities recorded

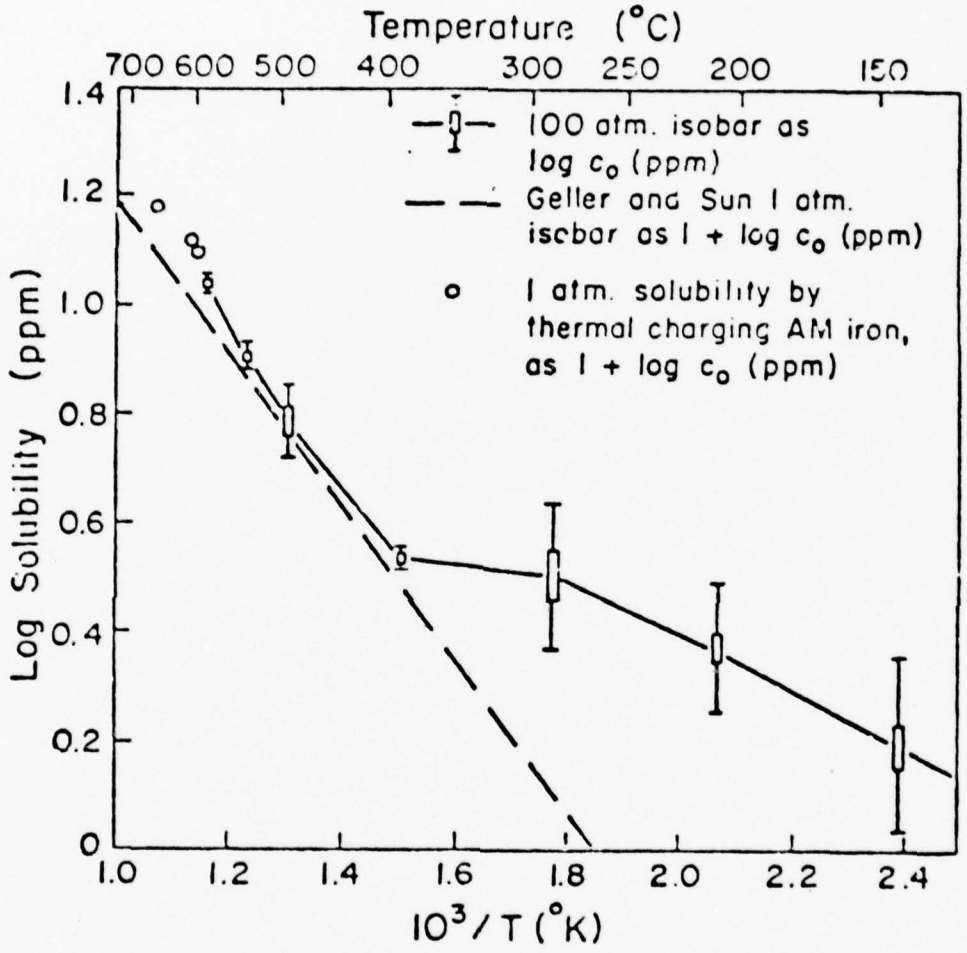

FIGURE 6: Solubility of Hydrogen in Iron Versus Inverse Temperature[32]

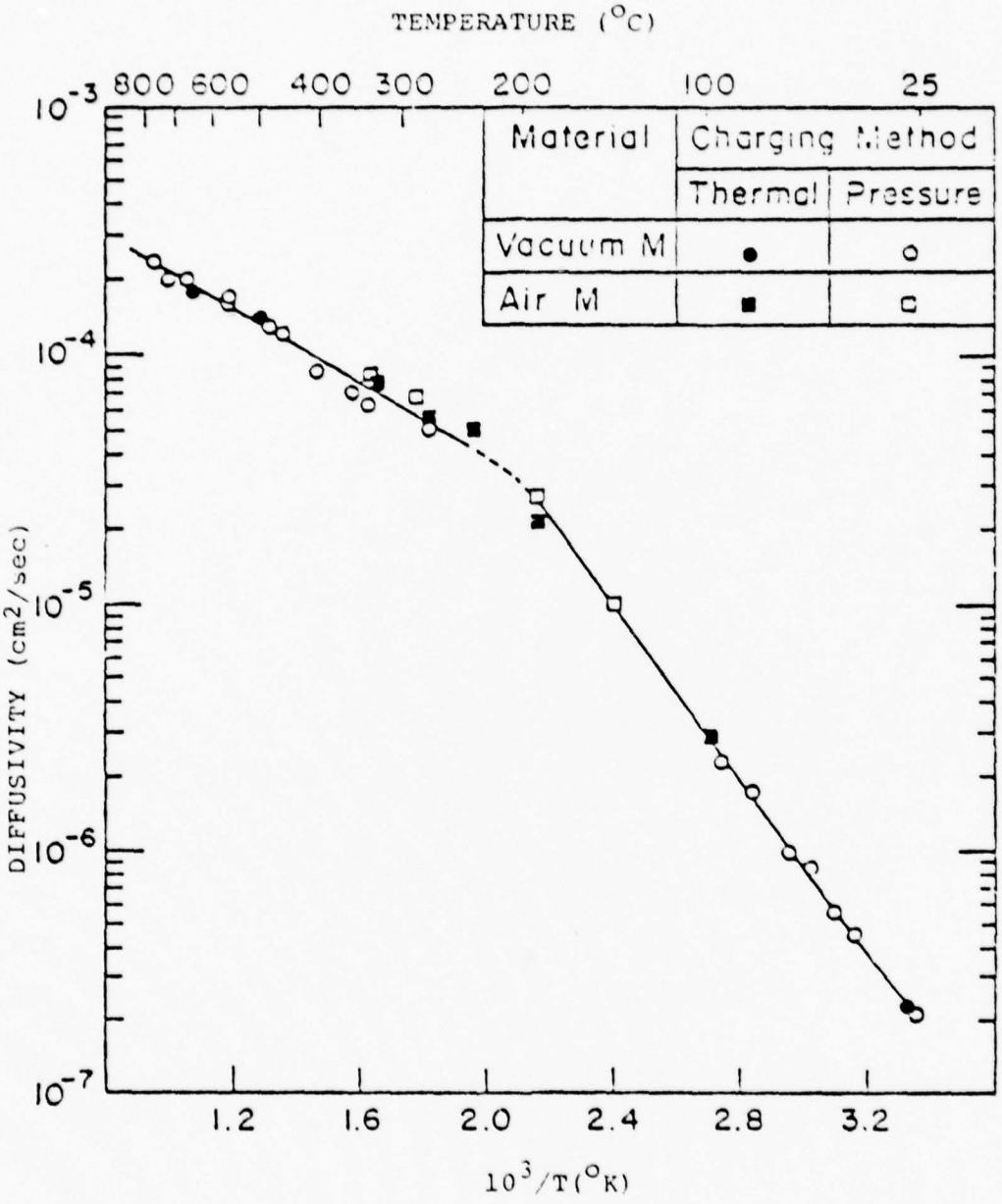

FIGURE 7: Diffusion Coefficient of Hydrogen in Iron Versus Inverse Temperature[17]

using evolution experiments[17, 24] tend to be lower than tohse associated with permeability experiments[18, 28]. This suggests that some sort of trapping phenomenon is occurring with hydrogen at these lower temperatures.

Darken and Smith[33] first suggested hydrogen delay or trapping. They found that annealed material exhibited an evolution rate slower than the absorption rate for the same sample. They also found an increase in solubility of hydorgen with increasing plastic deformation. Subsequent annealing at 800^{o}C was found to decrease the solubility from that of the cold-worked state but did not return the material to its original hot rolled condition with respect to hydrogen solubility. Since Darken and Smith much work has been done on hydrogen trapping[17, 18, 34, 35].

The exact nature of trapping sites is unclear, although many alternatives have been proposed on the basis of experimental work[18]. Darken and Smith[33] described traps as imperfections in the lattice. Gibala[36] suggested that dislocations, voids and interfaces should be considered possible trapping sites.

Since there seems to be much confusion related to low temperature data, researchers should work in this area. It is possible that part of the scatter in available data can be related to different experimental techniques which seem to exist from laboratory to laboratory. Table 1 summarizes available low temperature data on hydrogen permeation in iron:

Table 1 Hydrogen Permeation Data for Iron

Source	Year	Material	Temp. (^{o}C)	Effective Diffusivity ($\times 10^{-5} cm^2/sec$)	Charging Medium	Calculation Method
Barrer[26]	1940	Iron	25	.004*	NaOH	t_L
Johnson and Hill[31]	1960	Ferrovac Iron	25	0.44	Vaccum Degassing	Evolution Rate
Kumnick and Johnson[49]	1974	Armco Iron	25	1.3	NaOH or Gas Phase	$t_{0.63}$
Shih[15]	1975	Zone Refined Iron	25	1.5	NaOH	$t_{0.83}$
Quick[28]	1976	Zone Refined Iron	25	0.34	Gas Phase	Unstated
Devanathan and Stachurshi[37]	1962	Armco Iron	25 $\pm$ 2	3.5 - 8.9	H_2SO_4 and NaOH	$t_{0.63}$
Bockris and Devanathan[63]	1962	Armco Iron	25 $\pm$ 2	8.3	Various	$t_{0.63}$
Beck, Brockris, McBreen, Nanis[27]	1965	Zone Refined Iron	25 $\pm$ 1	6.05	NaOH	Unstated

Table 1 (cont'd)

Source	Year	Material	Temp. (^{o}C)	Effective Diffusivity (x 10^{-5} cm^2/sec)	Charging Medium	Calculation Method
Beck, Brockris, McBreen, Nanis[27]	1965	Armco Iron	25 $\pm$ 1	6.02	NaOH	Unstated
Beck, Brockris, Genshaw and Subramanyan[64]	1970	Armco Iron	27	5.0	NaOH	$t_{0.5}$
		Armco Iron	80	9.0	NaOH	$t_{0.5}$
Namboodhiri and Nanis[38]	1972	Armco Iron	22	2.14 - 3.48	H_2SO_4	$t_{0.5}$
		Armco Iron	22	5.53 - 8.45	H_2SO_4	$t_{0.5}$
Shreir and Radhakrishnan[62]	1965	Swedish Iron	25	0.03*	H_2SO_4	t_L
Wach, Miodownick and Lackowiak[55]	1966	High Purity Iron	25	2.5*	Gas Phase	t_L
Choi[65]	1970	"Iron" (.0045C)	12 - 70	0.09-1	pH 6.4 Buffer Solution	Varying
Dull[3]	1976	Ferrovac E Iron	25	0.06	H_2SO_4	Unstated

* Lattice Diffusivity

D. Purpose

The purpose of this work is to better characterize hydrogen transport in iron by studying both concentration and thickness dependences of hydrogen permeation in iron in the vicinity of room temperature.

In previous work at the University of Rhode Island[43, 44] and at the U.S. Army Materials and Mechanics Center[48] using an electrochemical hydrogen charging technique, no final steady state hydrogen permeation flux was observed. A possible explanation for this could be trap nucleation and growth throughout the experiment[34]. The high hydrogen flux levels produced during electrochemical charging could have been the cause. The best alternative to lower the flux level was to initiate gas phase charging experiments. Presumably by charging at lower flux levels a steady state will be attained.

CHAPTER 2

EXPERIMENTAL

A. Equipment and Experimental Technique

The electrochemical hydrogen permeation technique was first introduced by Devanathan and Stachurski[37]. It was later refined by Bockris, Nanis, and co-workers at the University of Pennsylvania[38-42]. It has the advantages of simplicity, low cost of equipment involved and the possibility for measuring the effects of widely varying hydrogen fluxes on permeation rates of hydrogen through metals[43].

A schematic of the actual gas-phase charging experimental cell used in this research is shown in Figure 8. Experimental cells of this type have been reported in experimental permeation research conducted at Cornell University[18], the University of Pennsylvania[37], Ohio State University[66], and M.I.T.[43]. By using an experimental cell similar to those reported elsewhere a good comparison with reported data should be achieved. The electric circuit used in this research is shown in Figure 9.

The gas phase permeation cell was composed of two three-necked, spherical pyrex flasks which have volumes of 1,000 ml each. They were connected by glass joints which are grooved to take Buna-N o-ring. A pinch clamp held the joints, with the sample membrane between them. The exposed area was 1.55 cm^2.

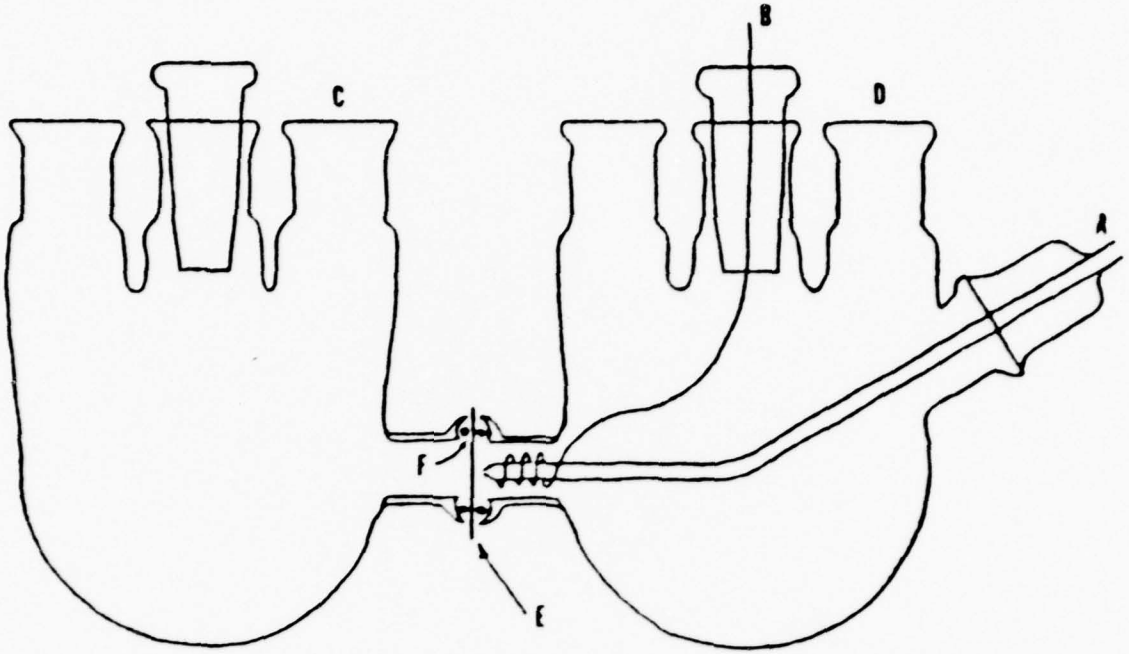

A Luggin Probe Reference Electrode
B Platium Counter Electrode
C Hydrogen Gas Inlet/Outlet
D Sparging Gas Inlet/Outlet
E Sample Membrane
F O-ring

Figure 8: Experimental Cell used for Gas Phase Charging

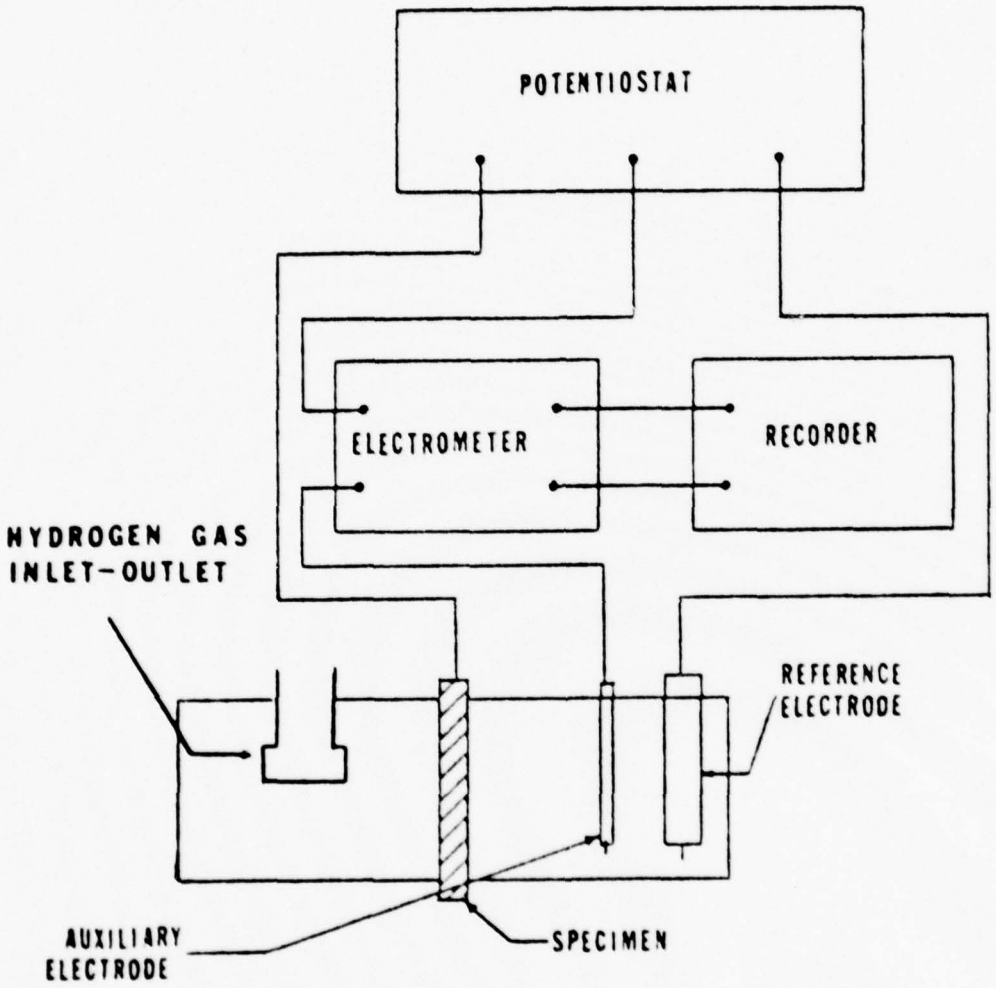

Figure 9 Schematic of Experimental Gas Phase Cell and the Electric Circuit Necessary for Gas Phase Charging Hydrogen Permeation Experiments.

The entry side of the sample membrane was exposed to hydrogen either from the gas phase or by cathodic polarization. On the exit side the amount of hydrogen that permeated through was measured as a function of time. The hydrogen was measured electrochemically by maintaining the exit side of the specimen at a constant anodic potential of + 250 mv versus a saturated calomel reference electrode. At this potential any hydrogen reaching the exit side would be ionized. A potentiostat supplied the current necessary for hydrogen ionization without changing the potential of the sample. The potentiostatic current was a direct measure of the amount of hydrogen leaving the exit side of the specimen. This current was recorded as a function of time with a Keithley Electrometer Model 600B and a Houston Omniscribe strip chart recorder. Since the sample had a constant cross-sectional area, the recorded current could be converted to current density. Using Faraday's Law of Electrolysis, current density can be expressed as hydrogen flux by the following relation[18]:

$$10^{-6} \text{ amp/cm}^2 = 1.04 \times 10^{-11} \text{ moles H/cm}^2\text{sec}$$

Fluxes can be measured accurately as low as 10^{-13} moles H/cm^2sec using this technique[18].

Gas phase charging permeation experiments were run using hydrogen (99.999%) which was mixed with argon (99.99%) with the aid of Matheson Model 7351 Gas Proportional Controllers. This mixture was simply allowed to

flow into the inlet side of the cell. By varying the flow rates of these two gasses different hydrogen partial pressures were attained. The total gas pressure in the cell was maintained at slightly over one atmosphere in all experiments.

The solution in the exit cell was 0.2N sodium hydroxide. Other researchers[4, 37, 38, 62] have used sulfuric acid for this research, but sodium hydroxide is most commonly reported[15, 18, 27, 38, 40, 41, 44, 54, 57]. All sodium hydroxide solutions were made from Fisher certified ACS electrolytic grade sodium hydroxide pellets used with deionized - distilled water. The solution was always deaerated with nitrogen gas for twenty-four hours prior to use. The solution in the cell was stirred with the aid of a magnetic stirrer. Nitrogen gas (99.99% pure) was bubbled through all experimental solutions to aid in stirring as well as to purge any dissolved oxidizing gases. The entire experimental apparatus is enclosed in a constant temperature chamber maintained to with + 0.1^{o}C by the use of a RFL Industries Proportional Temperature Controller Model 70-115.

Two side by side identical experimental permeation set ups are used during each experiment inside the constant temperature chamber. This is to check reproducibility[43].

While most of the experiments to be discussed in this thesis used the gas phase charging system discussed above, some experiments were run using electrolytically charged

hydrogen. The experimental cell for these experiments is shown in Figure 10. The right-hand or exit side of the cell is similar to that shown in Figure 8. An additional electrode is added to the left-hand or charging side of the cell, and the sample and auxiliary electrode are connected to a constant current D.C. electric power supply. The charging side of the cell was filled with an deaerated 0.2N sodium hydroxide solution. Electrolytic hydrogen was produced by turning on the power supply at a pre-set charging current. The term current density, CD, will be used to describe the charging current and its units are ma/cm^2. A schematic of the electrochemical cell and its electric circuit for electrochemical charging is shown in Figure 11.

Glass experimental cells having geometries similar to that shown in Figure 8 have been reported by a number of researchers[18, 43, 37, 45, 48], but early research at the U.S. Army Materials and Mechanics Research Center[48] and at the University of Rhode Island[43, 46] indicated a need for an improved electrochemical cell design incorporating the principles described by N. Greene[47] in his book on electrochemical technique. The recommendations of Greene were incorporated in the cell design shown in Figure 10[46].

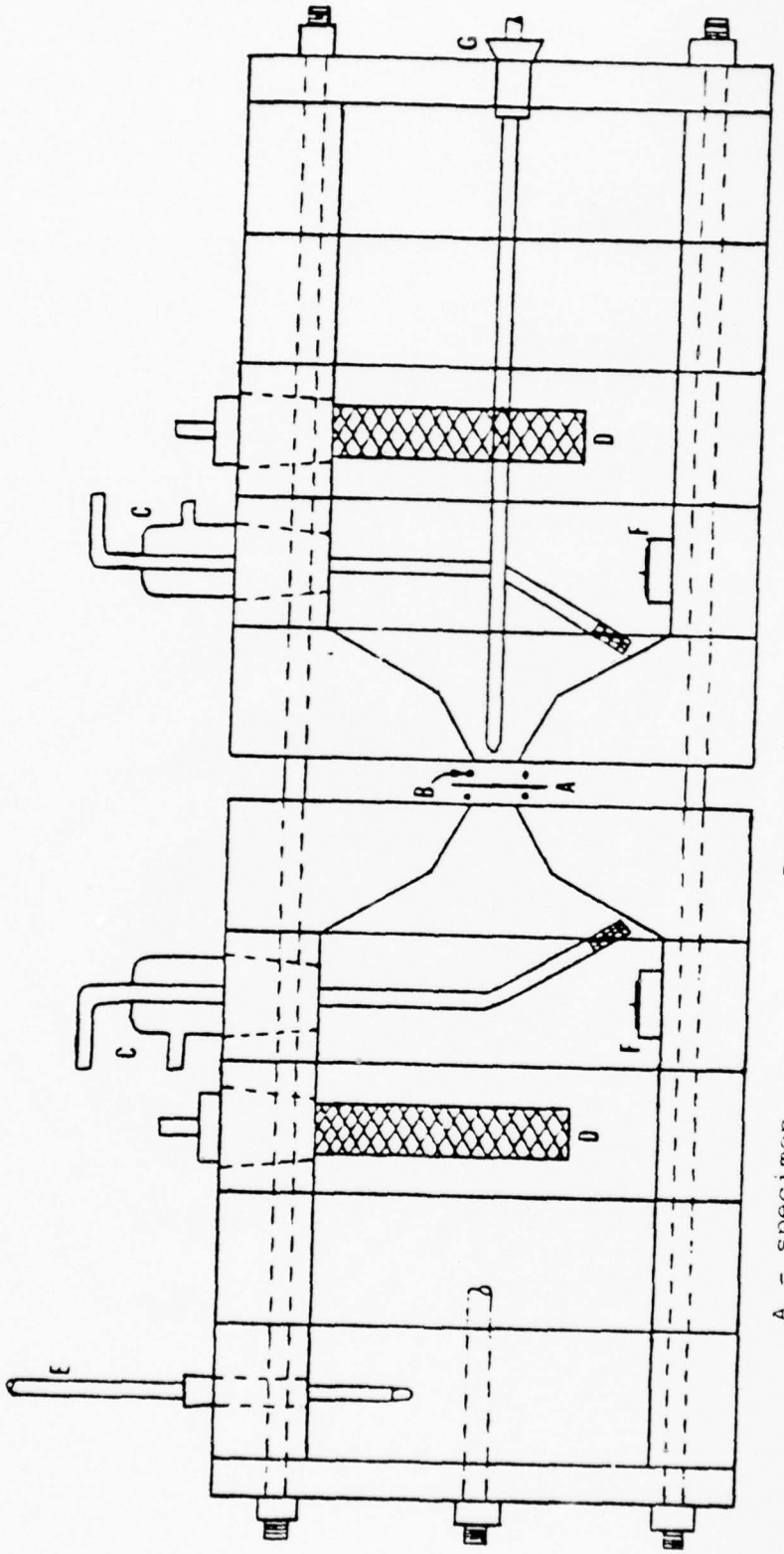

Figure 10: Experimental Cell used for Electrochemical Charging

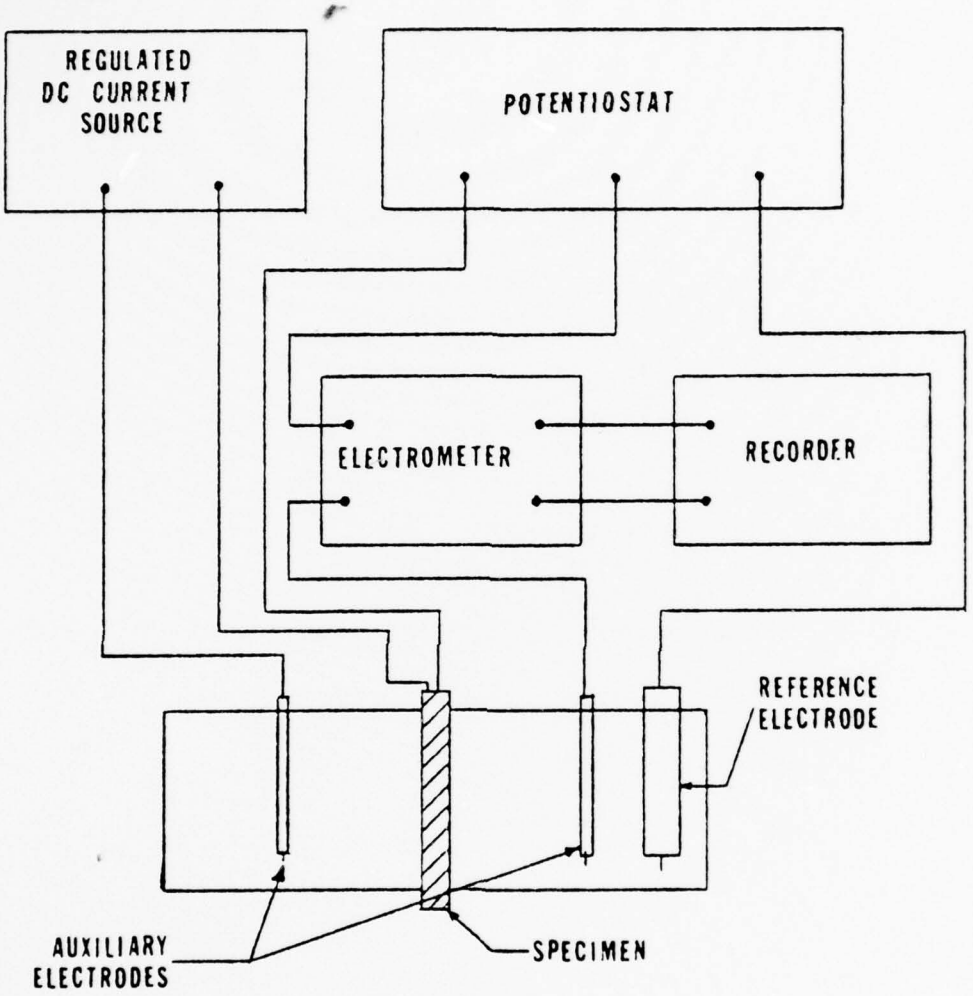

Figure 11 Schematic of Experimental Electrochemical Cell and the Electric Circuit. Necessary for Electrochemical Charging Hydrogen Permeation Experiments.

B. Sample Membranes

1. Material

The material chosen for this study was Ferrovac - E iron. The composition is shown in Table 2.

The metal was supplied in the as rolled condition 15.24 cm (6 in.) by 8.23 cm (3.25 in.) by 8.23 cm (3.25 in.). The as received iron was machined into sample sizes. This was done by first cutting the iron bar, perpendicular to the long axis of the bar, into slices of the appropriate thickness. These slices were then cut into four samples, each one being 2.54 cm (1 in.) x 2.54 cm (1 in.) x sample thickness.

Ferrovac - E iron was chosen in this research because of its high purity. Also permeation transients showed reproducibility from duplicate samples, something a previous study using Armco iron at the University of Rhode Island lacked. The impurities listed in Table 2 should not have a great effect on the permeation of hydrogen in this high purity iron[44].

There are hydrogen traps in the Ferrovac - E iron studied. All samples should have similar trap densities. The effect traps have on hydrogen permeation should exist in all experiments. This is supported by the fact that reproducibility was exhibited from duplicate samples.

Ferrovac - E iron[3, 15, 17, 29, 32] as well as Armco iron[18, 28, 33, 35, 43, 44, 46, 49] have been used by other researchers.

Table 2 Composition of Ferrovac - E Iron used in this Study*

Element	Weight %
Aluminum	0.01
Carbon	0.005
Chromium	0.001
Cobalt	0.002
Copper	0.002
Managanese	0.001
Molybdenum	0.005
Nickel	0.007
Phosphorus	0.003
Silicon	0.006
Sulphur	0.005
Tin	0.004
Tungsten	0.01
Vanadium	0.004
Oxygen	0.0078
Iron	Balance

* Analysis supplied by Colt Industries, Crucible Inc., Speciality Metals Division, Pittsburgh, PA.

2. Specimen Preparation

a. Polishing

The as received Ferrovac - E iron was machined to thicknesses varying from 0.051 cm (0.020 in.) to 0.208 cm (0.080 in.) by the procedure mentioned previously. Then a surface preparation sequence was performed. The square samples were ground with Carbimet - SiC grinding paper - down to 600 grit. The next stage was rough polishing including a 6 micron diamond abrasive polish followed by an 1 micron aluminum oxide abrasive polish. The samples were then ultrasonically cleaned in Buehler Ultramet Sonic Cleaning Solution for 30 minutes. A distilled water rinse was used to remove all residual cleaning chemicals, and a very shiny surface resulted. At the end of the preparation sequence the sample surface was checked for scratches by the use of a Unitron Inverted Metallurgical Microscope Model MEC-CM-055. This sequence was found to be quite reproducible from sample to sample.

b. Electroplated Palladium Surfaces on Iron Membranes

Examination of the potential-pH diagram for iron, Figure 12, (which has been experimentally confirmed)[50, 51], indicates that surface reactions (ion buildup and passive film formation) resulting in hydrogen blocking effects are expected in most aqueous solutions. During gas phase charging the inlet surface is not in an aqueous solution but in an oxidizing atmosphere. The iron would form an

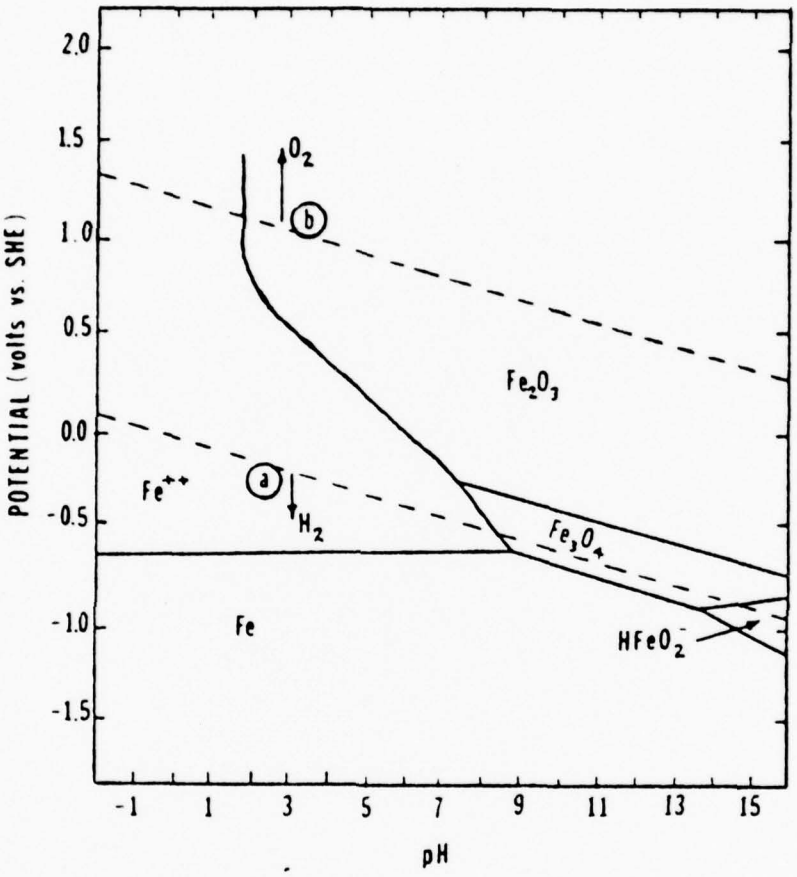

Figure 12: Pourbaix Diagram for Iron[45]

oxide film blocking hydrogen entry. Because of these blocking effects it was found to be necessary to coat the sample surfaces with an inert coating[43].

Palladium was chosen to coat the sample surface and is intended to produce an inert surface, minimizing corrosion effects on hydrogen entry, while supplying a readily permeable medium which is not rate controlling for hydrogen transport. Examination of the potential-pH diagram for palladium[50], Figure 13, indicates that palladium surfaces should be thermodynamically stable in most aqueous environments. The coating on the exit side of the sample is necessary to protect the surface from corrosion resulting from the applied potential used to ionize the hydrogen exiting the sample.

A previous study at the University of Rhode Island indicated the importance of obtaining an adherent palladium coating[43, 46]. Electroplated palladium was found to produce the most adherent surface.

Figure 14 shows the electroplating set up. The sample was attached to the negative output of a D.C. power supply and made the cathode, while platanized niobium was used as anodes. The electroplating solution was Technic Palladium RT*. The plating solution was gently stirred by a magnetic stirrer. The sample was immersed in the solution for controlled times and current densities. The Ca-

* Purchased from Technic Inc., Providence, R.I.

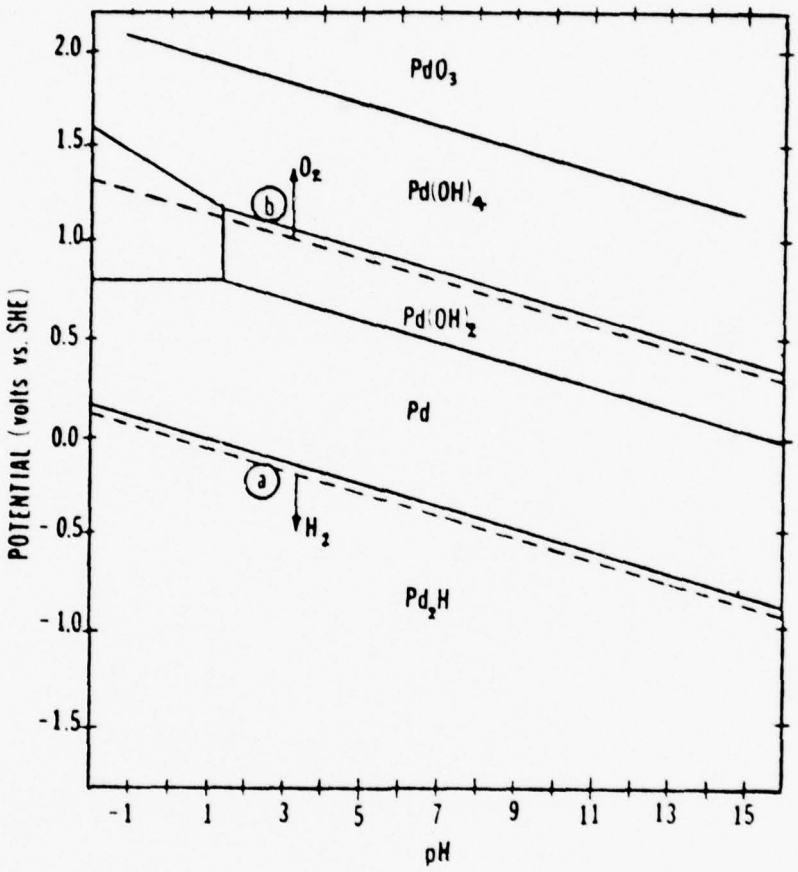

Figure 13: Pourbaix Diagram for Palladium[45]

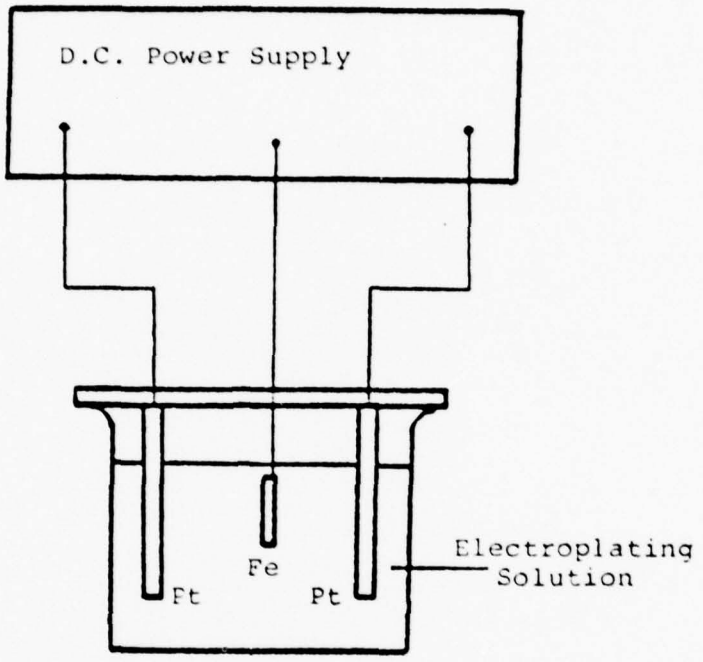

Figure 14: Electroplating Apparatus for Plating Palladium on Both Sides of the Sample Membrane

thodic current density was 55 ma/cm^2 and plating time was 2 minutes for 2000 A^o of palladium on each side. The plating time was 4 minutes when 4000 A^o of palladium was desired. As the sample was removed after being electroplated it was washed with distilled water and was then ready for a permeation experiment. All data in this report is for samples with 2000 A^o of electroplated palladium on both sides unless otherwise stated.

When palladium was necessary on only one side of the sample one of the anodes was removed and that side of the sample was masked with Scotch Electroplating Tape Number 470.

The sample surface remained bright and shiny after the electroplating process. Sample surfaces were microscopically checked before and after exposure. No damage was visible on either the inlet or exit surface.

Figure 15 shows a hydrogen permeation sample which was used in earlier hydrogen permeation studies at the University of Rhode Island[43]. The type of damage that might have occurred if this plating process had not been successful is quite apparent.

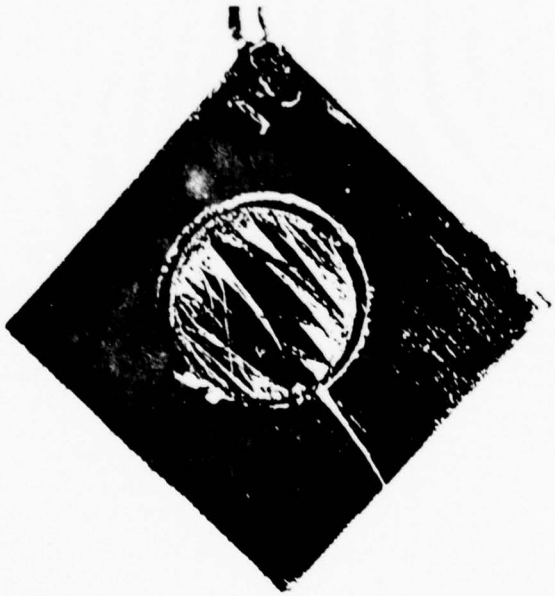

Figure 15: Palladium Coating Debonding on Entry Surface of Vapor Deposited Palladium Coating on Armco Iron Substrate. Sample was Exposed to 2.5 ma/cm^2 Cathodic Charging in 0.2N NaOH[43].

CHAPTER 3

RESULTS AND DISCUSSION

A. Experimental Parameters

1. Palladium Entry and Exit Surfaces

It is important to show that the palladium exerts no limiting effect on hydrogen transport during the permeation experiments. This is the same as showing that the bulk iron is the rate limiting material for hydrogen transport. Inlet and exit surfaces were both coated with palladium films. This was shown to be necessary by results which will be presented later in the text. The palladium does not measurably alter the transport of hydrogen because it is very thin, on the order of 10^{-5} cm, and because the palladium has a higher solubility for hydrogen than iron has for hydrogen[18].

An analysis of diffusion in composite membranes has been carried out by Barrie et. al.[52]. It shows that diffusion through the bulk iron is the rate limiting step. From Barrie et. al. the equation for permeation through a Pd-Fe-Pd composite membrane is:

$$\frac{L}{P_T} = \frac{L_{Fe}}{D_{Fe}\, S_{Fe}} + \frac{2L_{Pd}}{D_{Pd}\, S_{Pd}} \qquad (4)$$

and

$$\frac{L}{P_T} = \frac{L_{Fe}}{D_{Fe}\, S_{Fe}} + \frac{L_{Pd}}{D_{Pd}\, S_{Pd}} \qquad (4a)$$

for a Fe-Pd membrane.

where:

P_T = Permeability through composite material

D_{Fe} = Lattice diffusivity of hydrogen in iron

D_{Pd} = Lattice diffusivity of hydrogen in palladium

S_{Fe} = Lattice solubility of hydrogen in iron at equilibrium with 1 atmosphere hydrogen pressure

S_{Pd} = Lattice solubility of hydrogen in palladium at equilibrium with 1 atmosphere hydrogen pressure

L_{Fe} = Thickness of iron layer

L_{Pd} = Thickness of palladium layer

$L = L_{Fe} + 2L_{Pd}$ or $L_{Fe} + L_{Pd}$ = Total thickness of membrane

Oriani[14] found the lattice diffusivity of hydrogen in iron at 25°C to be 3.2×10^{-5} cm^2/sec, while Ansell et. al.[53] found the lattice diffusivity of hydrogen in palladium at 25°C to be 3.1×10^{-7} cm^2/sec. From Oriani[19] and Salmon[15] the ratio of lattice solubilities of hydrogen in iron and palladium at 25°C can be estimated as:

$$\frac{S_{pd}}{S_{Fe}} = 1.4 \times 10^{6} \qquad (5)$$

If a substitution is made into Equation 4 for the thinnest sample, $L_{Fe} = 6.1 \times 10^{-2}$ cm (0.024 in.) and $L_{Pd} = 2 \times 10^{-5}$ cm (2000 A°), using the fastest reported lattice diffusivity of

hydrogen in iron, Oriani's value, and the slowest reported lattice diffusivity of hydrogen in palladium, Ansell's value, it can be shown that the overall permeation process will be controlled by the bulk iron to with 2 parts in 10^7. As the thickness of the iron sample increases, the palladium will show even less influence on hydrogen transport[54]. This analysis therefore shows the worst effect the palladium could have on the overall permeation process. This sort of analysis has been used by other researchers[15, 18, 28, 54]. Thus palladium surface coatings can be used on iron permeation samples with no measurable change in the total transport rate.

2. Typical Data and Reproducibility

A typical experimental permeation curve has distinct regions, which are shown in Figure 16. First is the breakthrough region which describes the time necessary for the first hydrogen to leave the exit side. The measured breakthrough time is dependent upon diffusivity, the sensitivity of the measuring system and the thickness of the membrane. Second is a transient region which shows an increasing hydrogen flux with time. The transient region is followed by a steady state region associated with a stable hydrogen concentration profile within the membrane. The magnitude of the steady state flux depends on the lattice diffusivity, the concentration of lattice hydrogen at the entrance surface and the thickness of the membrane, as shown by Fick's first law[13]:

$$J_{\infty} = D_L \frac{C_o}{L} \qquad (6)$$

which can be rewritten as:

$$D_L = \frac{J_{\infty}}{C_o L^{-1}} \qquad (6a)$$

where:

J_{∞} = Steady state hydrogen flux

D_L = Lattice diffusivity

C_o = Concentration of lattice hydrogen at entrance surface

L = Membrane thickness

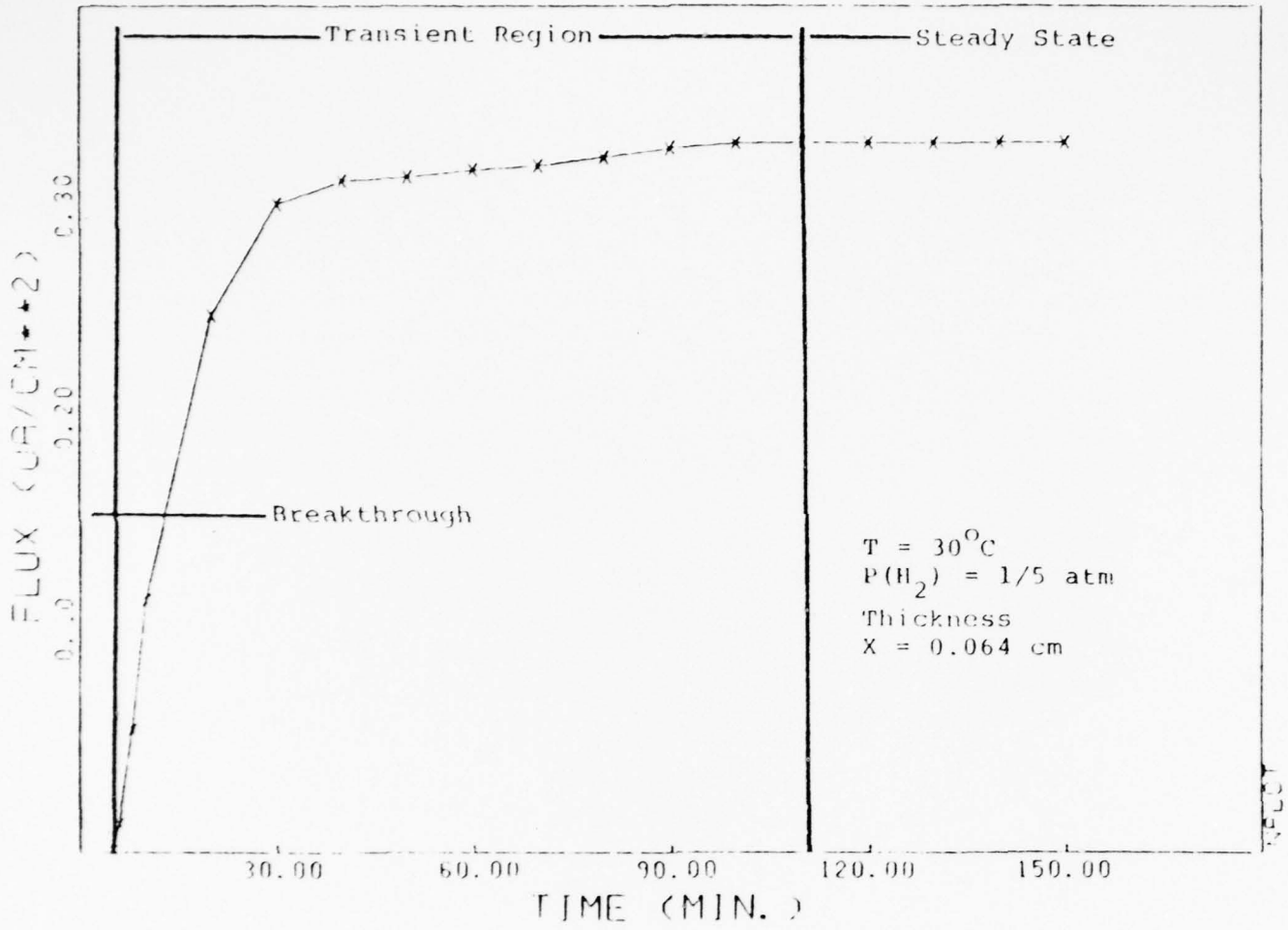

Figure 16: Typical Absorption Transient.

If the hydrogen source is turned off at the inlet surface, an evolution transient is observed at the exit surface as shown in Figure 17.

Successive absorption and evolution transients recorded on the same sample show good reproducibility as is shown in Figures 18 and 19. This reproducibility suggests that traps are not being formed or enlarged during hydrogen charging, at least within the sensitivity of the technique to measure trap growth. Similar reproducibility has been demonstrated at the University of Pennsylvania[27, 34], Cornell University[18, 49], and at U.C.L.A.[3] using electrochemical charging. The necessity to precharge samples with hydrogen, presumably to fill all hydrogen traps, has been observed necessary to obtain reproducibility in consecutive charging experiments[3, 17, 31, 32, 55, 56]. This necessity was not noted in the present research.

Bockris and Subramanyan[34] suggested that hydrogen induced damage occurs in metals at high hydrogen flux levels due to trap nucleation and spreading of microcracks formed by dislocation buildups. Since gas phase charging (low hydrogen flux) was used in this research, internal damage may be minimal.

The times necessary in this research for the permeation curve to level off or reach steady state are considerably longer than times reported elsewhere[3, 4, 15, 18, 49]. The times to steady state reported elsewhere range from 10 minutes down to 1 minute[3, 4, 15, 18, 49]. These research-

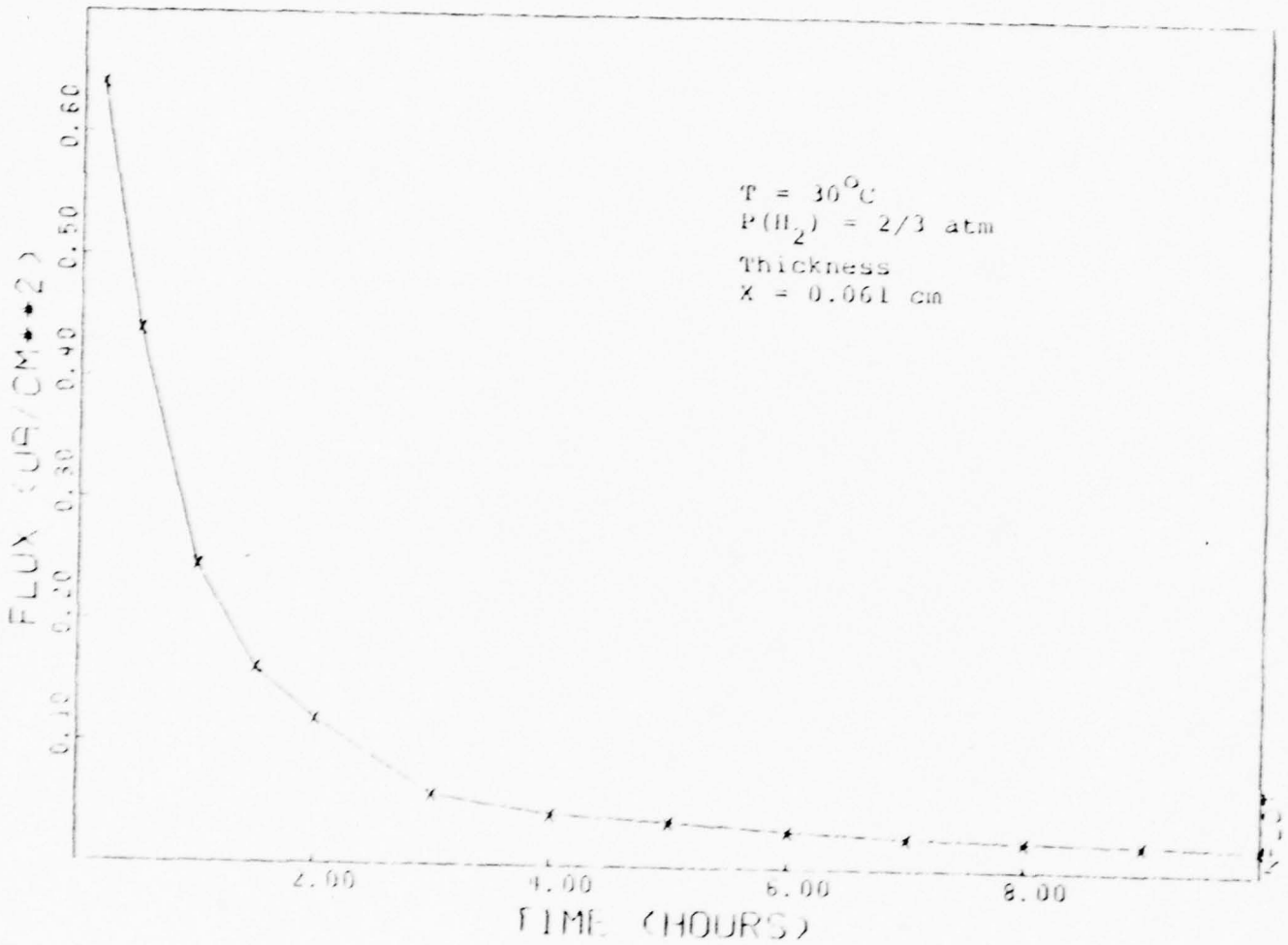

Figure 17: Typical Evolution Transient.

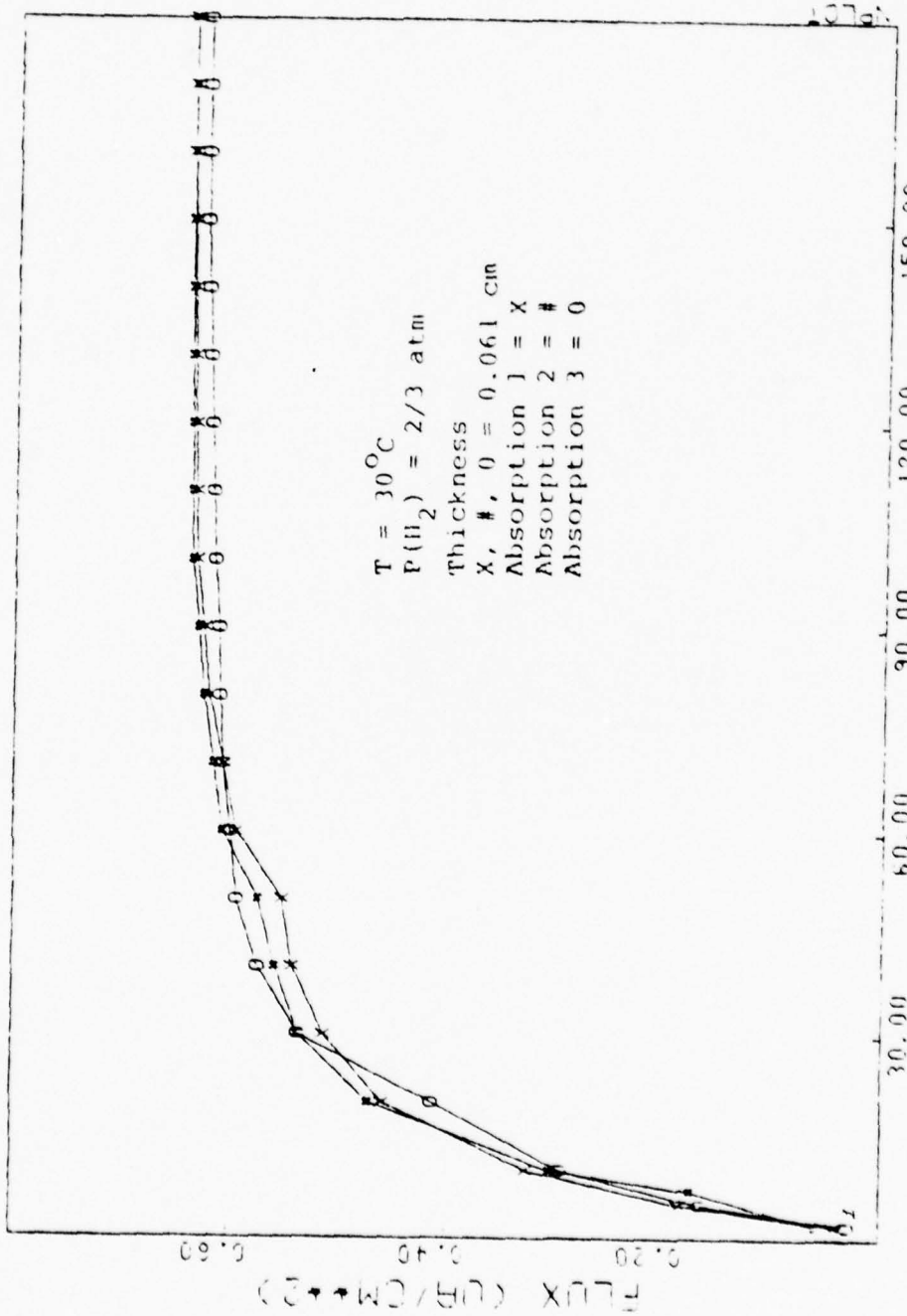

Figure 18: Successive Absorption Transients.

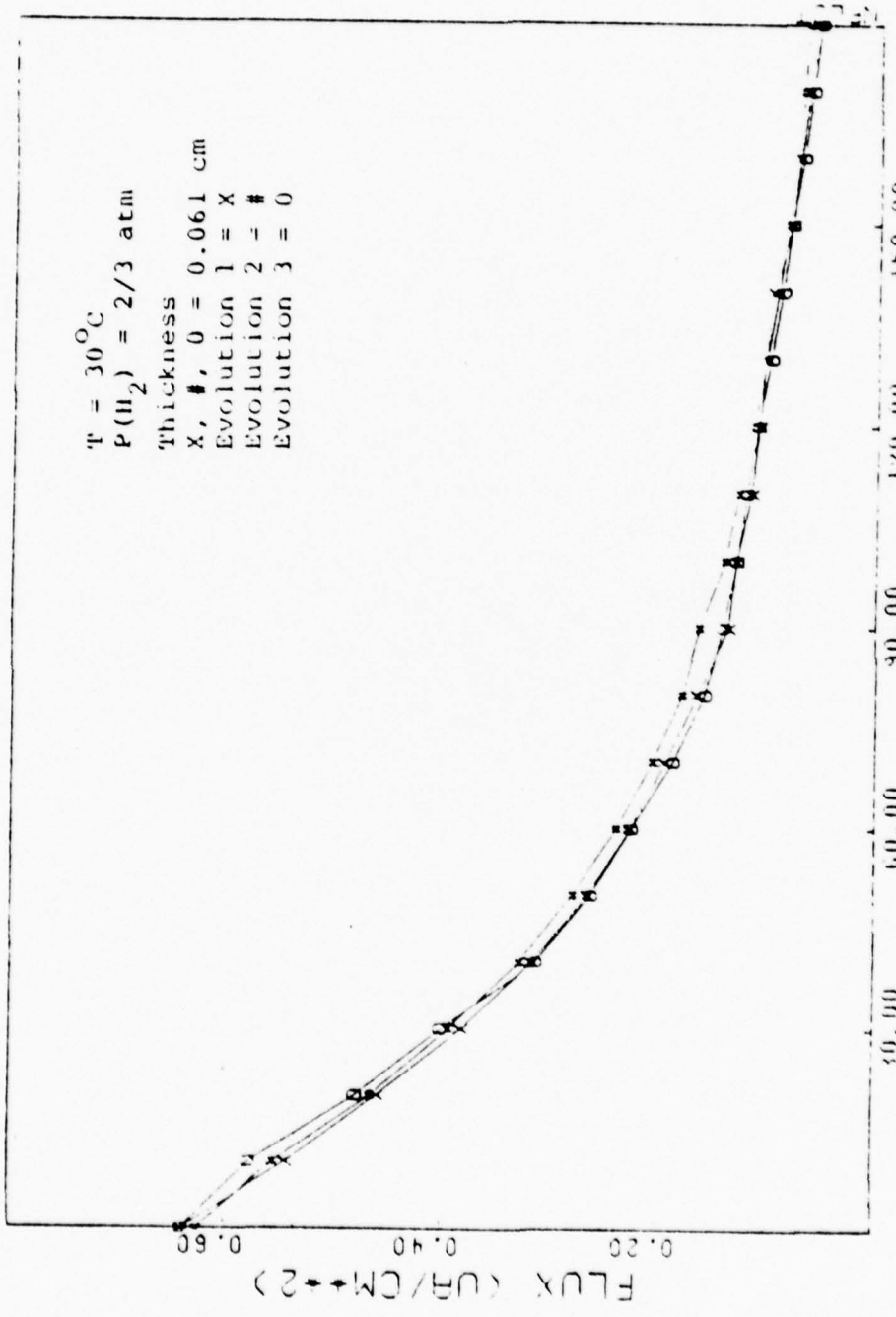

Figure 19: Successive Evolution Transients.

ers do not show the permeation transients for a long term situation, say 10 hours. In this study a steady state was reached in most cases in less than 5 hours, but in a few cases steady state was not attained until 10 hours.

Non-steady state conditions have been reported by other researchers[3, 4, 34] and were the subject of an extensive earlier investigation at the University of Rhode Island[43, 46].

3. Surface Versus Volume Control

In permeation experiments it is important to consider the possibility of surface impedence[18]. Stated otherwise bulk transport should be the controlling factor not surface entry processes. A suitable test is the measurement of the steady state flux as a function of membrane thickness, Fick's First Law[3, 15, 18, 24]. Following the relation in Equation 5 the steady state flux, J_∞, should vary linearly with inverse thickness, L^{-1}. Figure 20 is a plot of steady state flux versus inverse thickness, and it shows a linear relationship for three hydrogen partial pressures, indicative of a bulk transport controlled process.

Absorption curves for membranes of different thicknesses are shown in Figures 21-23. The basic shapes of the permeation curves remained the same throughout all experiments done via gas phase charging.

It was stated earlier in this thesis that the necessity to coat the samples with electroplated palladium existed. Experiments were run to varify this. When a sample with an uncoated (bare) inlet surface but coated exit surface was tested in a gaseous hydrogen environment, no permeation flux was recorded. A plausable explanation for this is that the inlet surface reactions were not allowing hydrogen to enter the iron. These surface reactions could include an iron oxide layer build-up which would hinder hydrogen entry. Yet, when an uncoated exit side and coated inlet side sample was tested, a permeation flux was

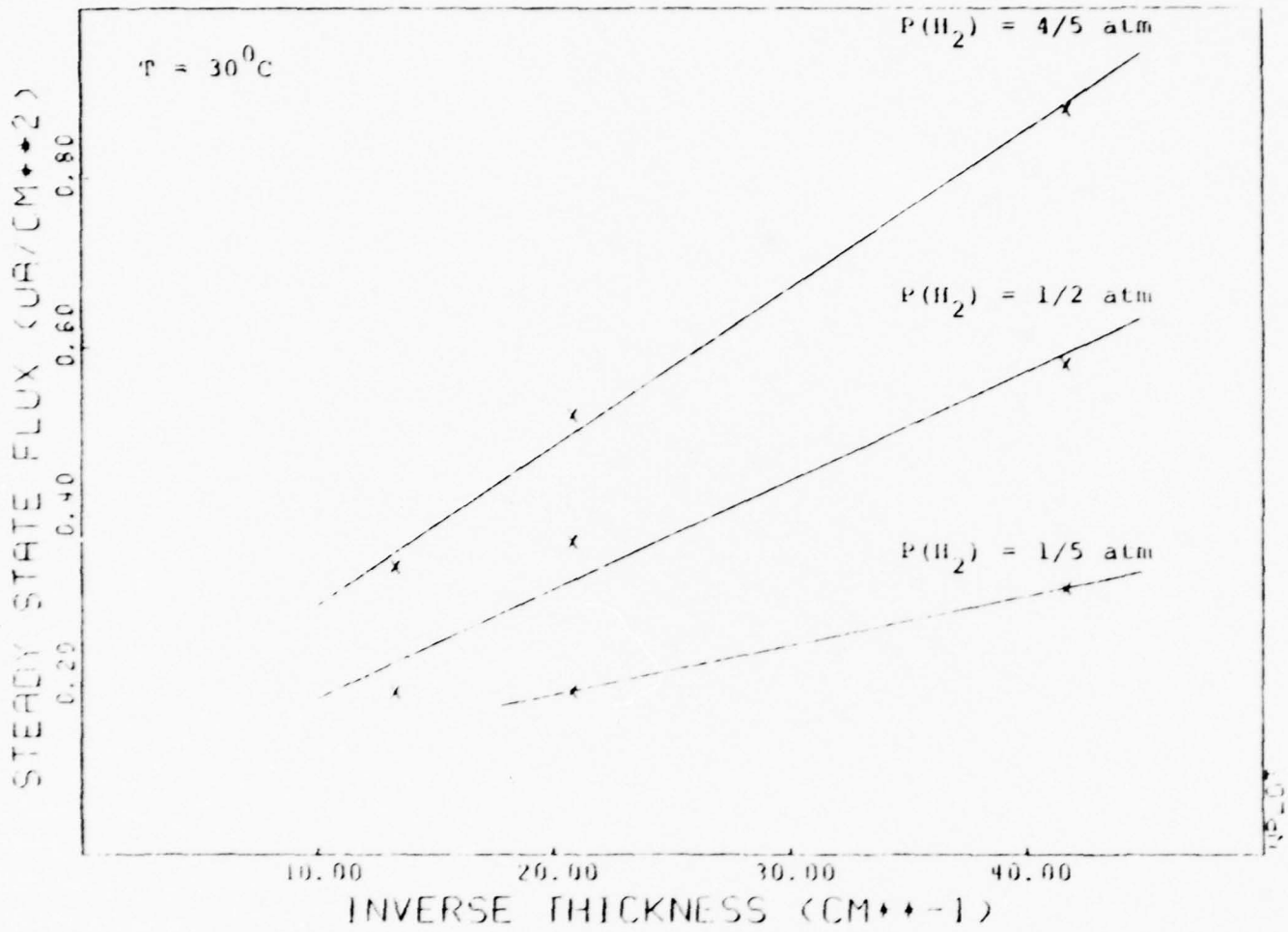

Figure 20: Steady State Flux as a Function of Sample Membrane Thickness.

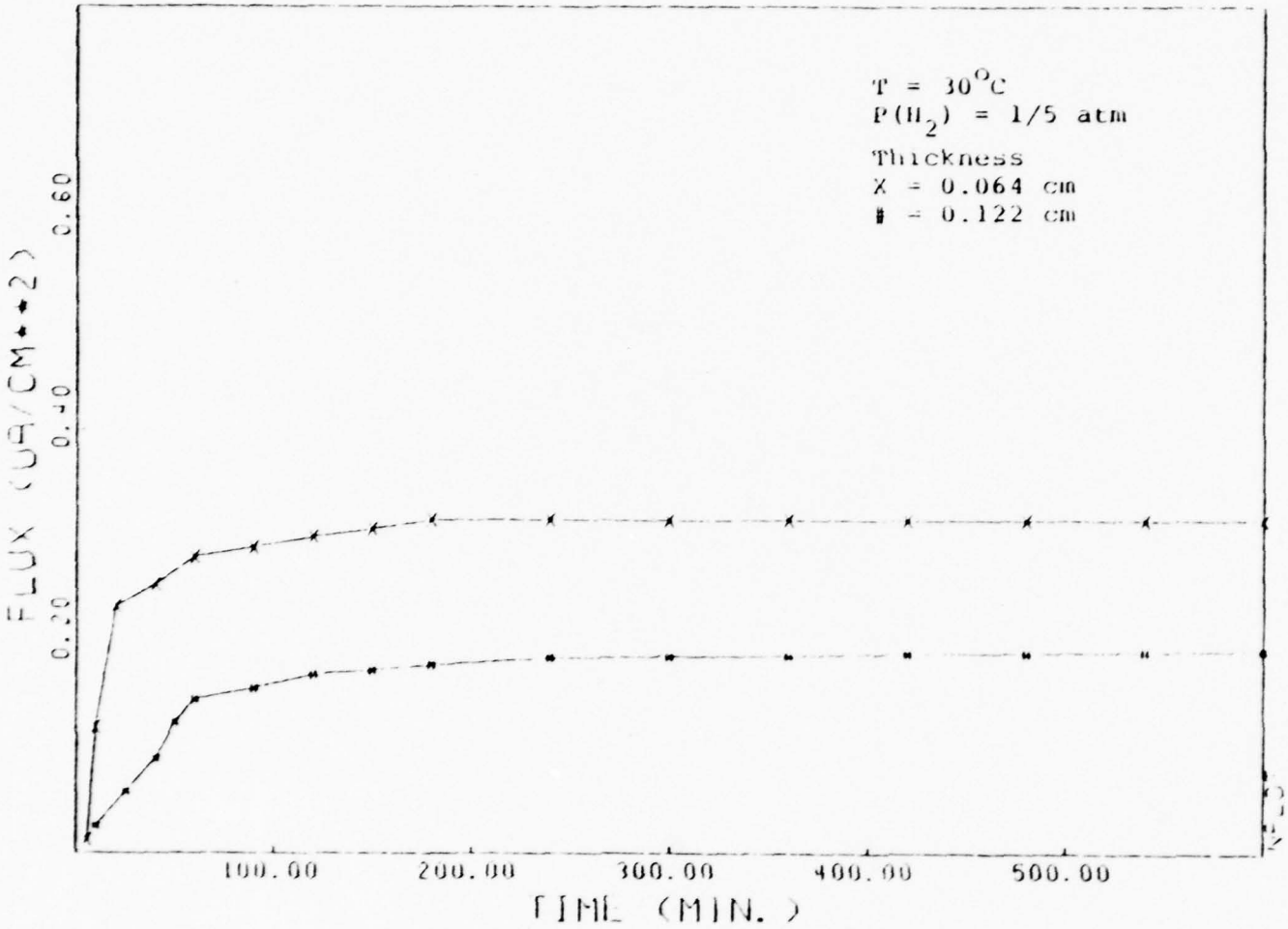

Figure 21: Absorption Transients as a Function of Thickness at a Hydrogen Partial Pressure = 1/5 atm.

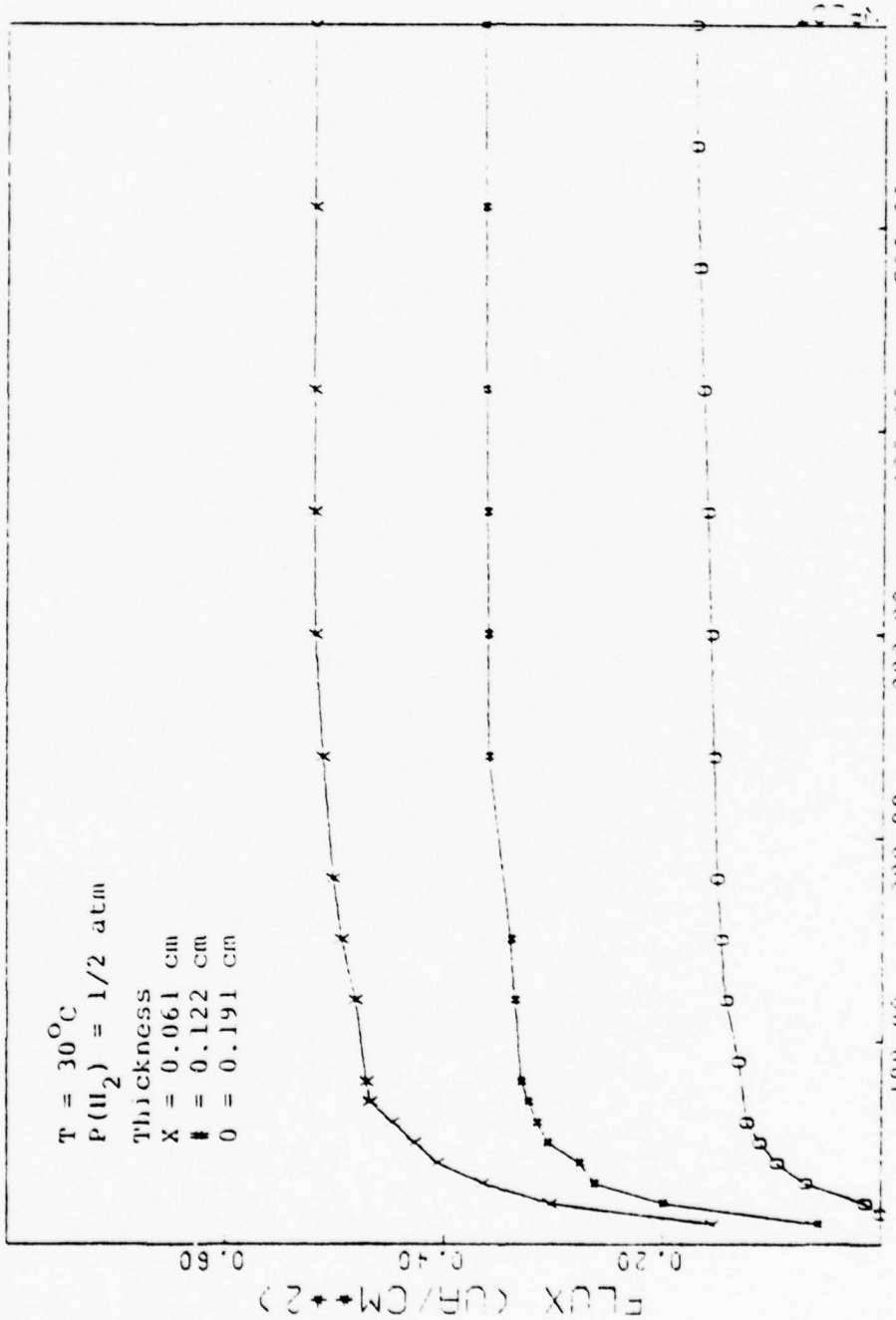

Figure 22: Absorption Transients as a Function of Thickness at a Hydrogen Partial Pressure = 1/2 atm.

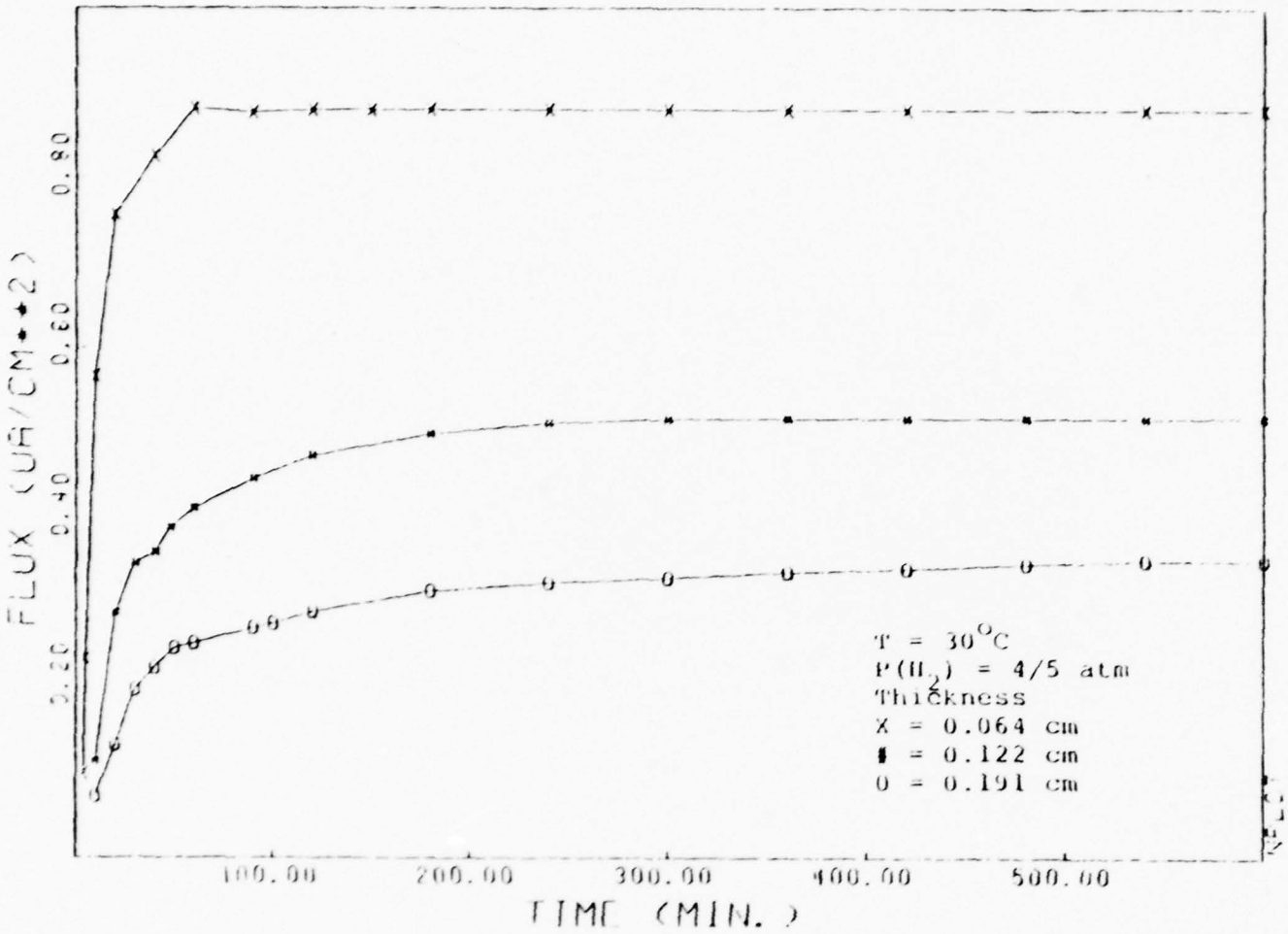

Figure 23: Absorption Transients as a Function of Thickness at a Hydrogen Partial Pressure = 4/5 atm.

registered. The reproducibility of this experiment is shown in Figure 24. But the recorded permeation flux was considerably lower than a coated inlet side and exit side sample under the same hydrogen partial pressure conditions, Figure 25. This lower permeation flux can be related to the build up of the iron oxide external layer in the prescence of the sodium hydroxide environment. The iron oxide stops the hydrogen from leaving the iron, causing the change in permeation curves seen in Figure 25.

Since the iron surfaces are coated with palladium, it is necessary to test for palladium thickness having any effect on permeation. Figure 26 shows a plot of permeation data for samples with varying palladium thicknesses. No appreciable difference in absorption transients was observed, thus proving palladium not having a measurable effect on permeation. This experimental data supports the calculation shown earlier in Section 3A1 of this report.

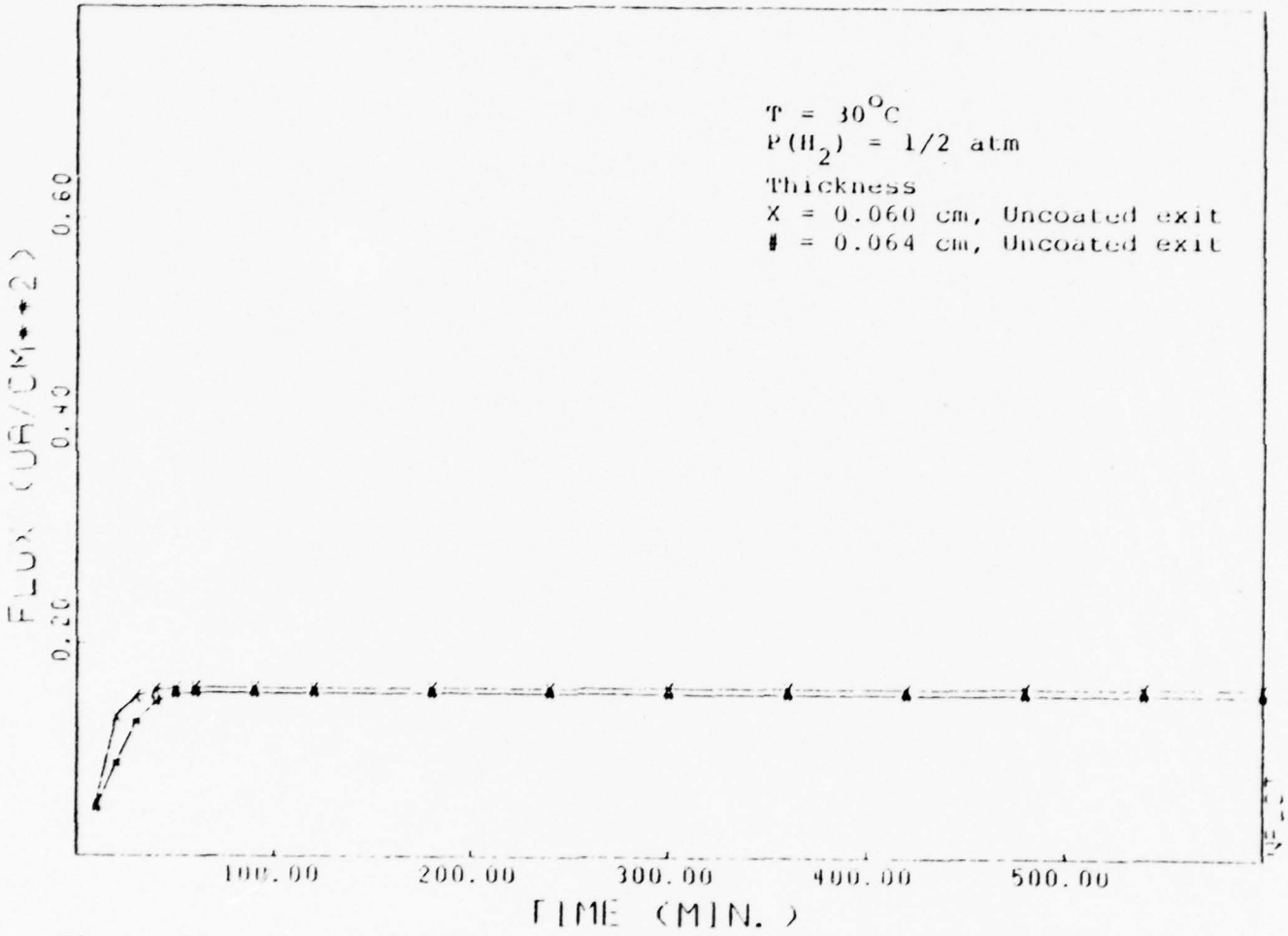

Figure 24: Absorption Transients Showing Reproducibility of Uncoated Exit Surface Permeation Transients.

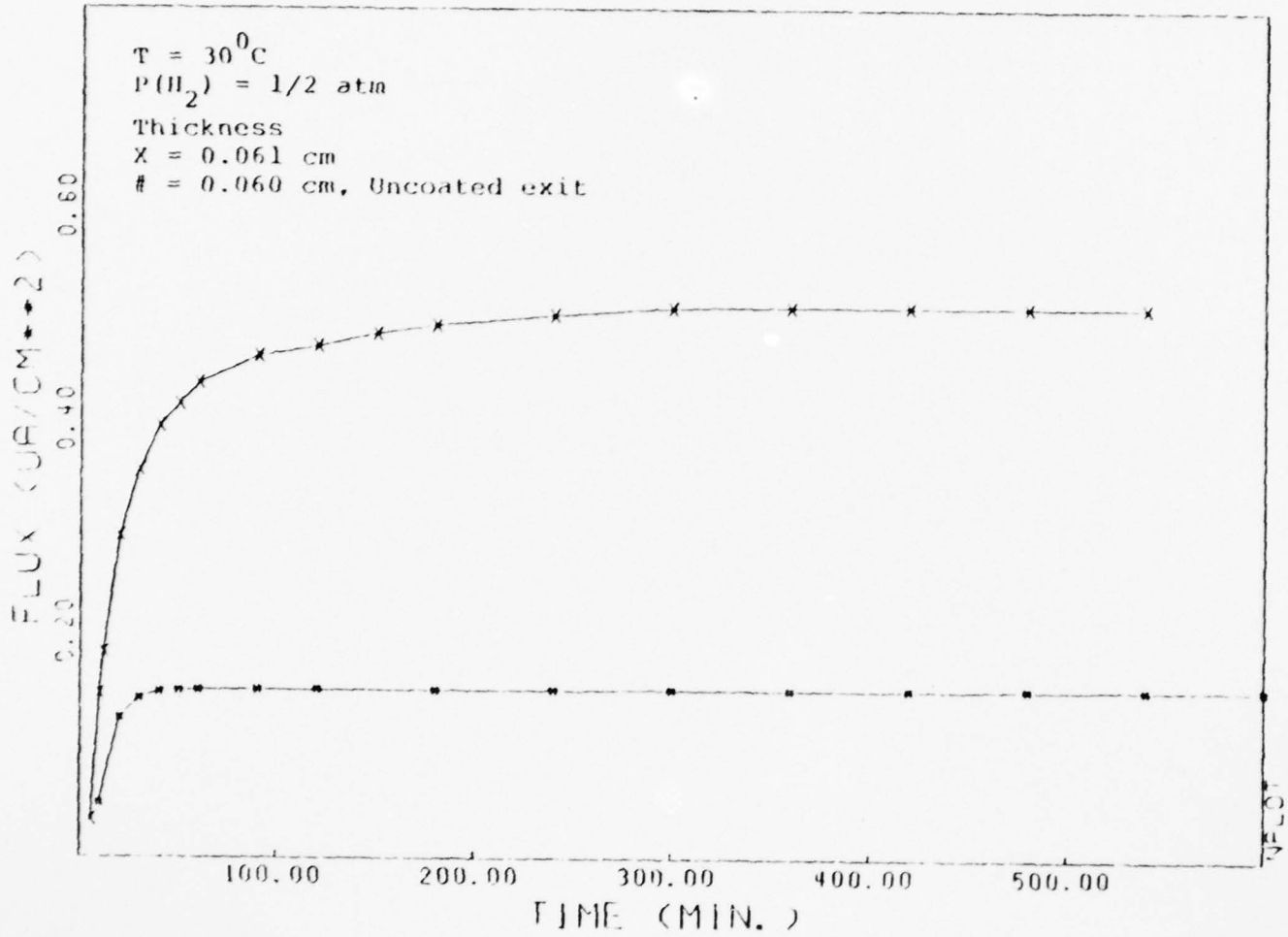

Figure 25: Absorption Transients Comparing Coated and Uncoated Sample Membranes.

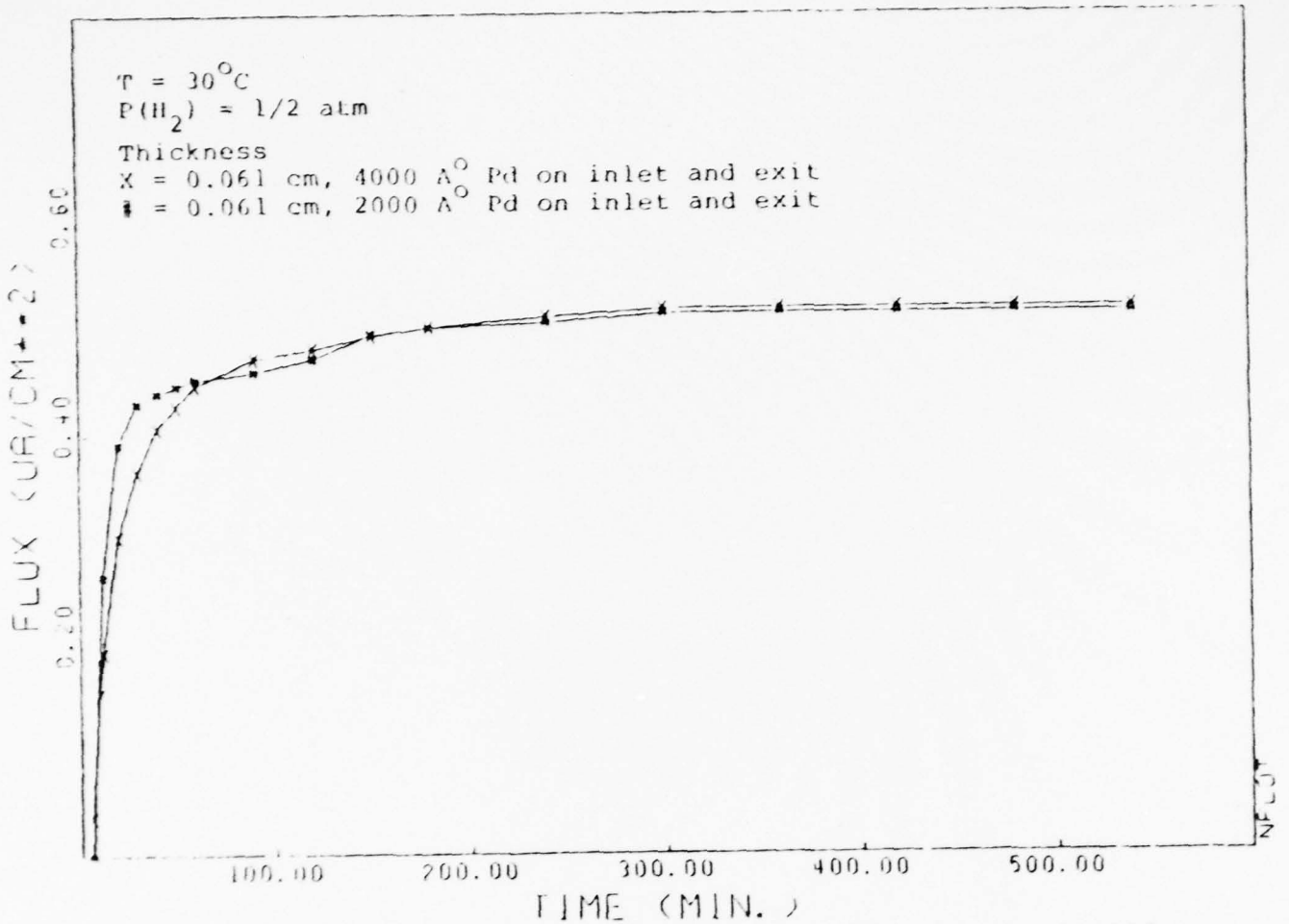

Figure 26: Absorption Transients Showing the Effect of Different Thicknesses of Palladium Coatings.

4. Electrochemical Charging Versus Gas Phase Charging

It was mentioned earlier in this thesis the fact that times to reach steady state flux were considerably longer than times reported elsewhere. No steady state flux was attained in previous studies at the University of Rhode Island[43, 44] and at the U.S. Army Materials and Mechanics Research Center[48] using an electrochemical charging method.

Figure 27 is a plot of a typical electrochemical charging experiment permeation transient. No steady state was attained after 100 hours. The charging current density was 0.025 ma/cm^2.

An attempt was made to compare electrochemical charging flux hydrogen levels so that of gas phase charging. Due to equipment limitations the comparison was not attained. The D.C. power supply used for production of electrolytic hydrogen could not produce a low enough output. The electrochemical hydrogen flux level is at least four times greater than the maximum gas phase hydrogen flux level achieved. The ability of compare electrochemical and gas phase charging has been reported by other researchers [15, 18, 28]. A possible explanation of the non-steady state condition could be continuous internal damage causing hydrogen trap growth[34]. This would be more apparent at higher hydrogen flux levels.

Since a steady state flux level was necessary for data analysis to produce diffusion coefficients or activation energies, gas phase charging was used in all experiments

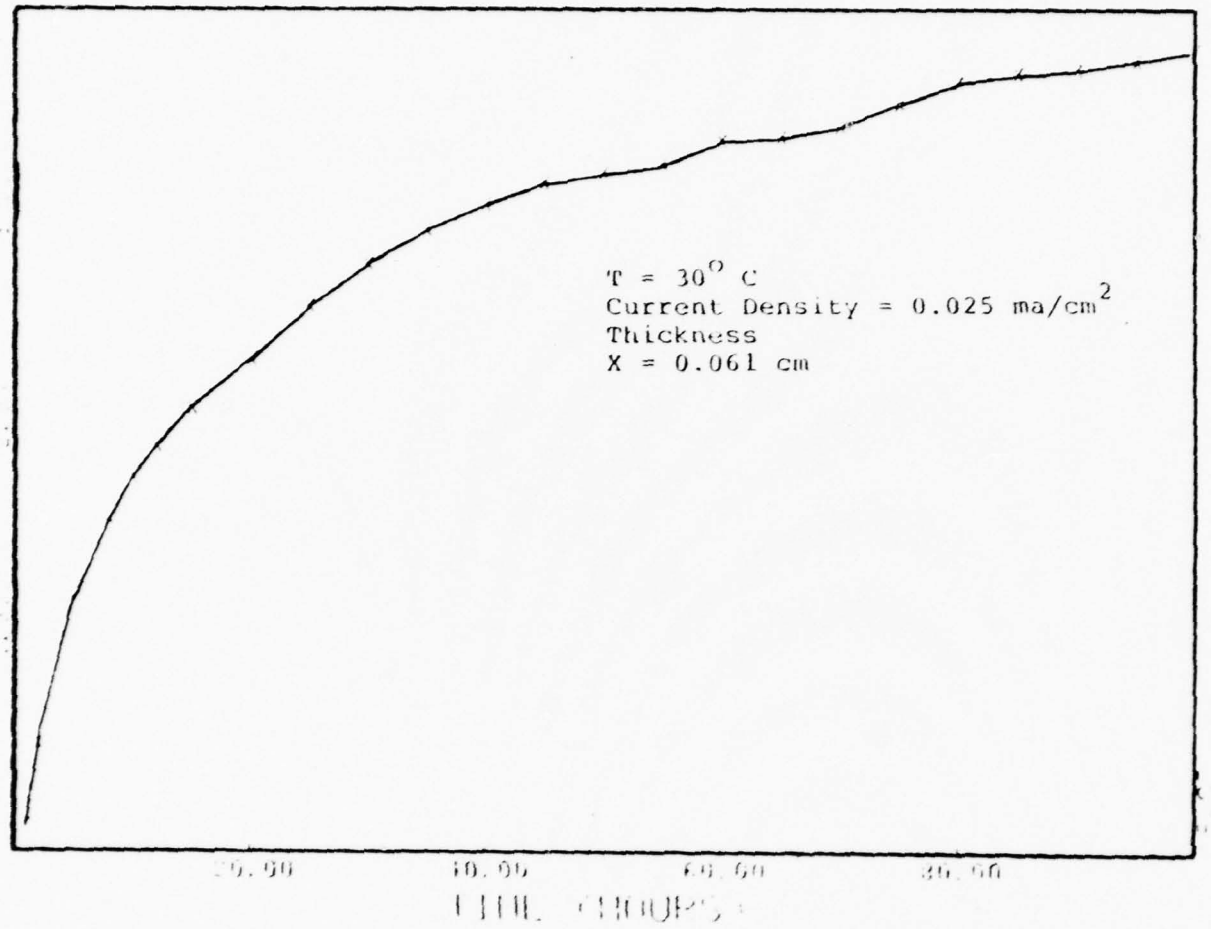

Figure 27: Typical Electrochemical Charging Transient.

where any diffusion coefficients were calculated.

B. Data Analysis Methods

1. Effective Diffusivity from Absorption and Evolution Transients

If the permeation of hydrogen in iron is diffusion controlled, the effective diffusivity of hydrogen in iron can be calculated under the assumption that hydrogen permeation obeys Fick's First Law[15, 18, 29]. McBreen et. al.[57] developed an analysis for hydrogen absorption that can apply to the permeation experiments done in this study. The permeation process can be shown by Fick's Second Law for constant diffusivity[57]:

$$\frac{\partial^2 C}{\partial x^2} - \frac{1}{D_L}\frac{\partial C}{\partial t} = 0 \qquad 0 < x < L \qquad (7)$$

where:

C = Concentration of hydrogen

t = Time

The boundary and initial conditions for this experimental set-up during an absorption transient are shown below[57]:

$C = C_o \quad X = 0 \quad t \leq 0$

$C = 0 \quad X = L \quad t \geq 0$

$C = 0 \quad 0 < X < L \quad t < 0$

Using the method of Laplace transforms on Equation 7 for the above conditions, a series solution of the transient hydrogen flux is obtained[57]:

$$J_T = \frac{2 D_L C_o}{\pi^{1/2} L} \frac{1}{(\tau)^{1/2}} \sum_{n=0}^{\infty} (-1)^n \exp -(2n + 1)^2/4\tau \quad (8)$$

where:

$$\tau = \frac{D_{EFF}\, t}{L^2} \quad (9)$$

J_T = Hydrogen flux at time, t

D_{EFF} = Effective diffusivity of hydrogen in iron

Noting from Equation 6 that:

$$J_\infty = \frac{D_L C_o}{L} ,$$

we have:

$$\frac{J_T}{J_\infty} = \frac{2}{\pi^{1/2}} \frac{1}{\tau^{1/2}} \sum_{n=0}^{\infty} (-1)^n \exp -(2n + 1)^2/4\tau \quad (10)$$

The first term of the series in Equation 10 gives results valid up to 96.77% attainment of steady state permeation, i.e.,

$$\frac{J_T}{J_\infty} = \frac{2}{\pi^{1/2}} \frac{1}{\tau^{1/2}} \exp -\frac{1}{4\tau} \quad ; \quad 0 < \tau < 0.5 \quad (11)$$

Using Equation 10, it possible to calculate effective absorption diffusivity of hydrogen in iron by finding the time required to attain any fraction of the steady state permeation up to 96.7%[57]. The equation for effective absorption diffusivity now reads:

$$D_{EFF} = \frac{\tau L^2}{t} \quad (9a)$$

For example, when the flux reaches 83% of its steady state value, the following expression for effective diffusivity is used.

$$D_{EFF} = \frac{0.25L^2}{t_{83\%}} \qquad (12)$$

where:

$t_{83\%}$ = Time necessary for permeation flux to reach 83% of J_∞

Figure 28 is a plot of dimensionless time, τ (Equation 9), versus normalized flux, J/J_∞. There seems to be very good agreement between actual data and theory, therefore the $t_{83\%}$ analysis is shown to be valid and is used in this permeation study.

The same sort of analysis used for absorption transients can be used for evolution transients[15, 18, 57]. Using the method of Fourier analysis, effective diffusivities can be calculated. However it is important to point out that because the boundary condition at the inlet surface is not well defined when hydrogen charging is stopped, the evolution transient analysis is somewhat more complicated[15, 18, 47].

The absorption transient analysis will be used in this thesis to calculate effective diffusivities. Thus the term "effective diffusivity" as used in this thesis is actually "effective absorption diffusivity."

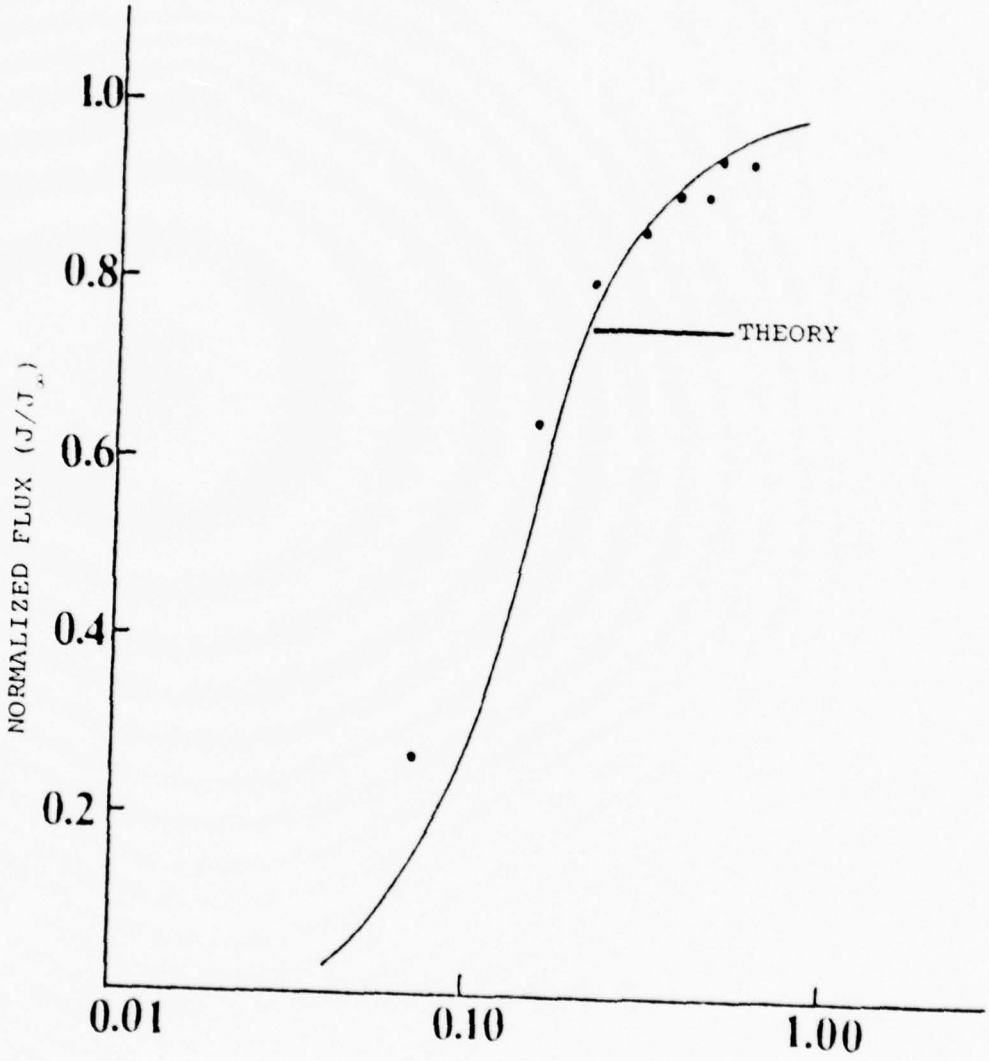

Figure 28: Comparison of Laplace Transform Prediction with Experimental Results.

Figure 29 is a plot of calculated effective diffusivity versus thickness at certain hydrogen partial pressures. It is shown that as hydrogen partial pressure is increased at the same thickness there exists an increase in calculated effective diffusivity.

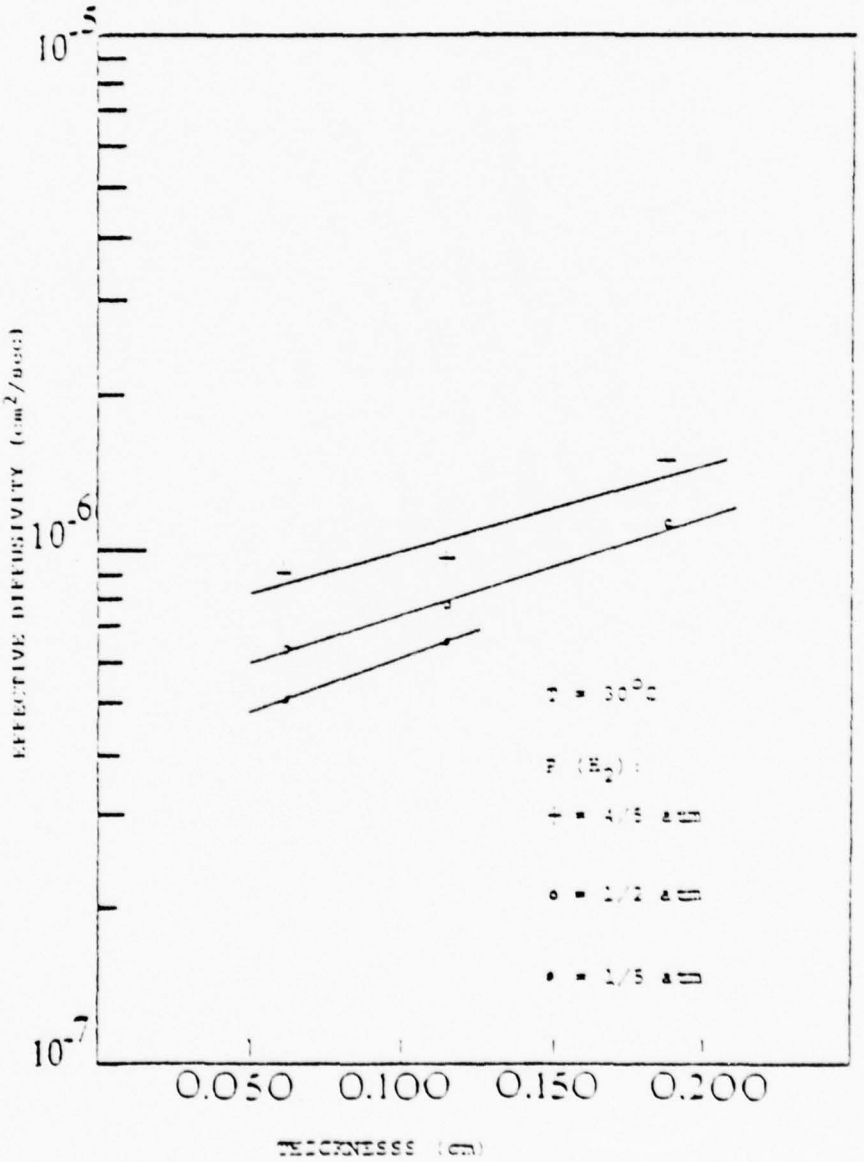

Figure 29: Effective Diffusivity as a Function of Sample Membrane Thickness.

2. Lattice Diffusivity from the Time Lag Analysis

Lattice diffusivity can be calculated from time lag extrapolations. Figure 30 shows an ideal time lag extrapolation. The value of the time lag, t_L, is derived from a plot of the total hydrogen flux versus time. What is meant by the total hydrogen flux is the total quantity of hydrogen emerging from the exit side, in other words the time integral of the permeation current. When a steady state permeation flux has been attained, the slope of this curve will be linear. The time lag is calculated by extrapolating this straight line back to the horizontal or time axis. McNabb and Foster in 1963 developed a time lag analysis to take into account the effect of hydrogen trapping, this was later modified by Boes and Zuchner[51] in 1976. Since this analysis was developed in 1963, earlier researchers could not take advantage of its simplicity.

McNabb and Foster[58] modified Fick's second Law to explain trapping as follows:

$$\frac{\partial C_L}{\partial t} + N_x \frac{\partial \theta_x}{\partial t} = D_L \nabla^2 C_L \qquad (13)$$

where:

D_L = Lattice diffusion or hydrogen

θ_x = Fraction occupancy of traps

N_x = Trap density

C_L = Lattice concentration of hydrogen

When considering rate of interchange of hydrogen atoms between trapped and diffusing species, the rate equation for

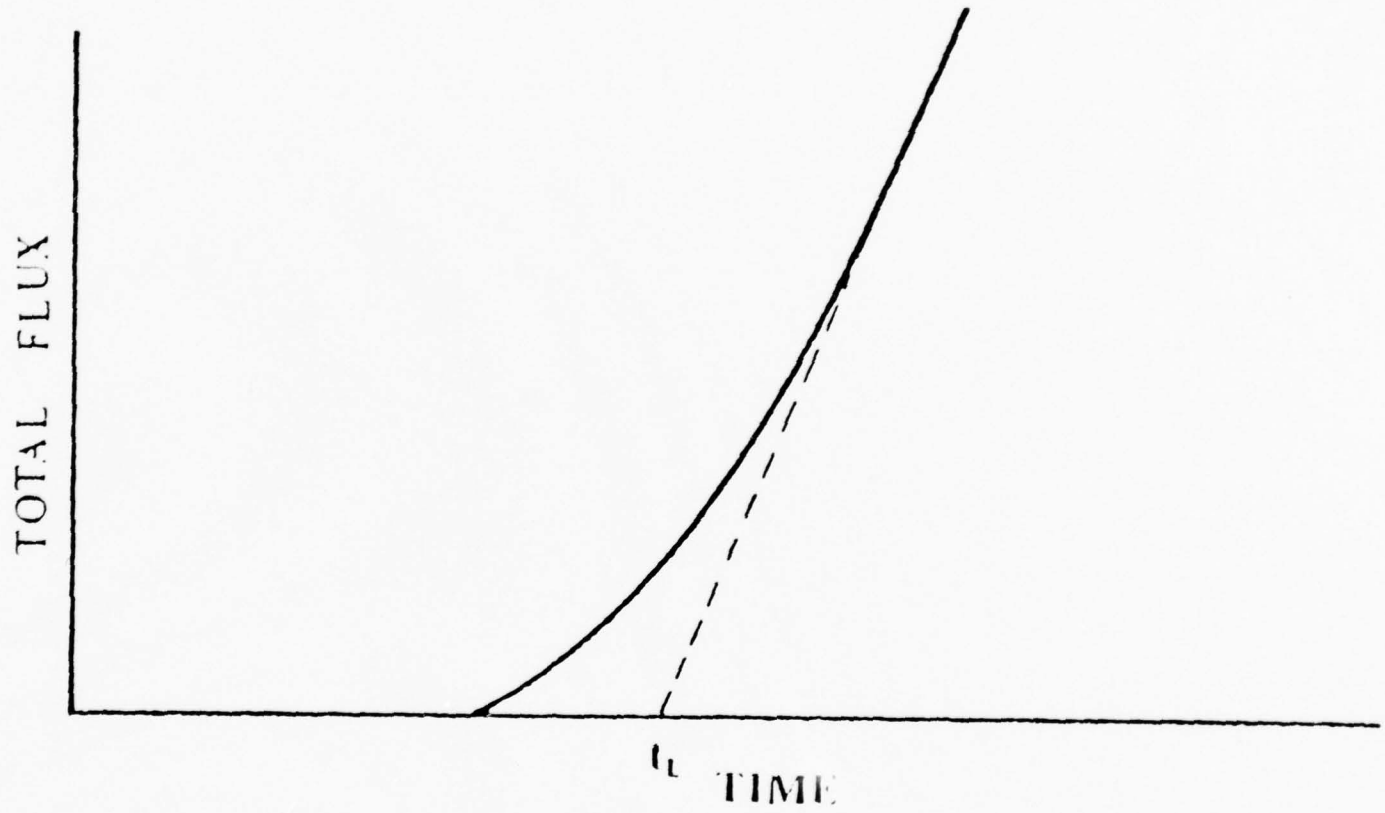

Figure 30: Ideal Time Log Extrapolation.

trapping is:

$$\frac{\partial \theta_x}{\partial t} = k\, C_L\, (1 - \theta_x) - p\theta_x \qquad (14)$$

where:

k = The kinetic trapping parameter

p = The kinetic releasing parameter

A solution of Equation (13) is used to desribed the lag time:

$$t_L = \frac{a^2}{D_L}\left[\frac{1}{6} + \frac{\alpha}{2\beta} + \frac{\alpha}{\beta^2} - \frac{\alpha}{\beta^3}(1 + \beta)\log(1 + \beta)\right] \qquad (15)$$

where:

a = Jump distance (membrane thickness)

$\alpha = N_x \frac{k}{p}$ = trapping parameter

$\beta = C_o \frac{k}{p} = \frac{\theta_x}{1 - \theta_x}$ = activity of hydrogen in traps

C_o = Lattice concentration at input surface of the permeation membrane

Only the first term of Equation 15 is used when a time lag analysis is necessary to calculate lattice diffusivity[59]. The rest of the terms in Equation 15 are negligible. The equation for time lag becomes:

$$t_L = \frac{1}{6}\frac{a^2}{D_L} \qquad (16)$$

or

$$D_L = \frac{1}{6} \frac{a^2}{t_L} \tag{16a}$$

Figure 31 is an actual time lag plot of a 0.122 cm (0.048 in.) thick membrane at a hydrogen partial pressure of 1/5 atm. The time lag is equal to 28 minutes. Substituting into Equation 16a a value for lattice diffusivity of 1.47×10^{-6} cm^2/sec is obtained.

Figure 32 is a plot of lattice diffusivity versus thickness for three different hydrogen partial pressures. There seems to exist an increase in calculated lattice diffusivity as thickness is increased.

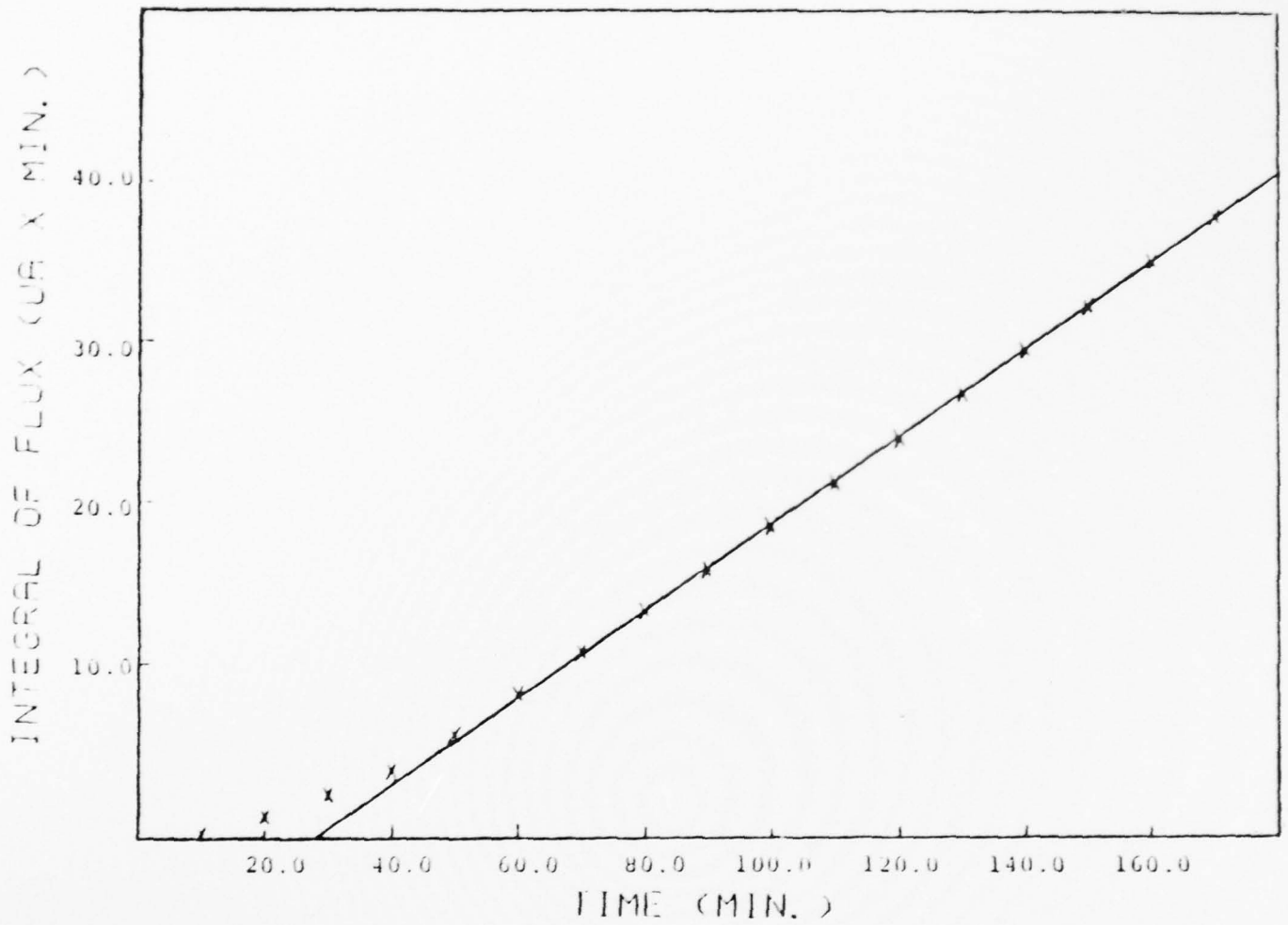

Figure 31: Actual Time Lag Extrapolation for the Permeation Transient Shown in Figure 21.

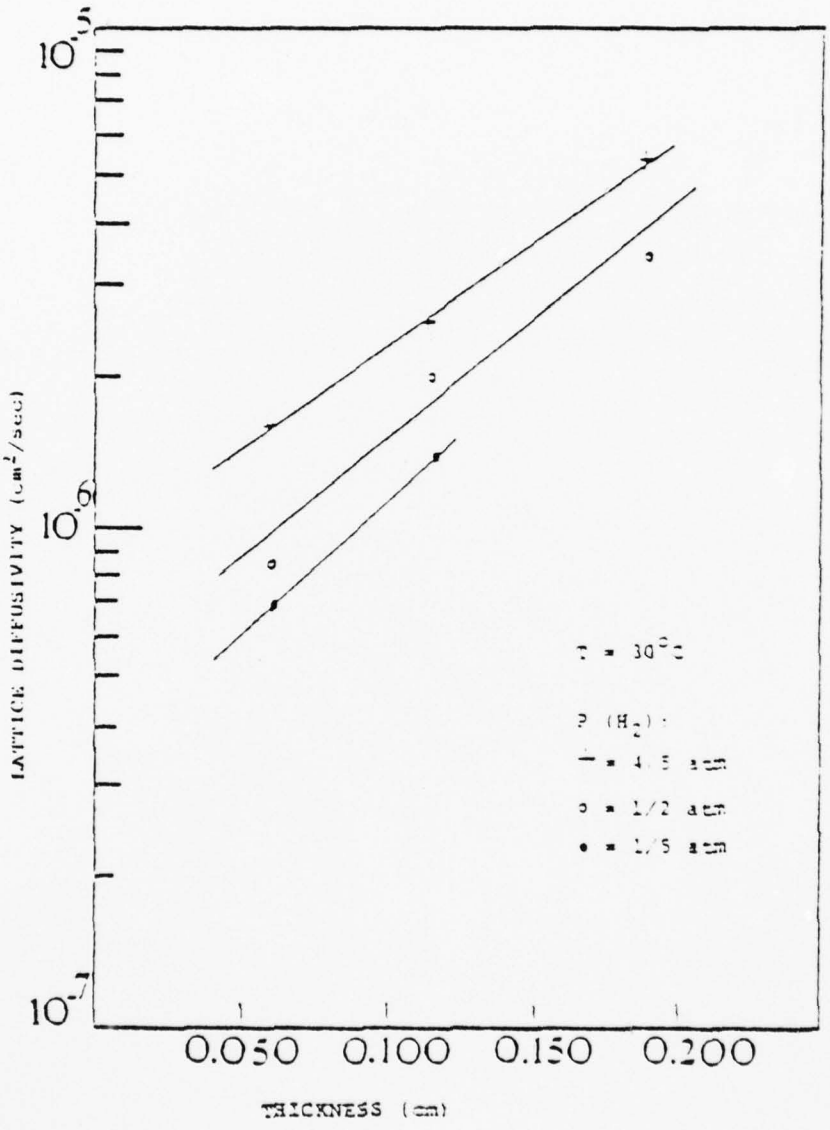

Figure 32: Lattice Diffusivity as a Function of Sample Membrane Thickness.

3. Temperature Effects on Permeation

The effect of temperature on permeation was studied. Figure 33 shows absorption curves for various temperatures. As temperature was increased, the value of steady state flux increased. The time necessary to obtain steady state flux also increased with increasing temperature.

A plot of calculated effective diffusivity versus reciprocal temperature is shown in Figure 34.

Restating Equation 3:

$$D_{EFF} = D_o \exp^{-Q/RT} \tag{17}$$

it is seen that this equation has the form of a typical reaction-rate equation first described by Arrhenius[60]. Taking the common logarithm (2.3 Log_{10} (x) - Ln Cx) of Equation 17 yields:

$$\text{Log } D_{EFF} = - \frac{Q}{2.3\ RT} + \text{Log } D_o \tag{18}$$

This is an equation of the form:

$$y = mx + b \tag{19}$$

which is the equation of a straight line. It can be seen that the relationship between Log D_{EFF} and 1/T is linear with its slope equal to -Q/2.3R. Activation energy, Q, can now be simply calculated. When this analysis is performed on a least squares fit of the data of Figure 34 it gives an activation energy of diffusion of 3.5 Kcal/mole. This value compares reasonably will with the high tempera-

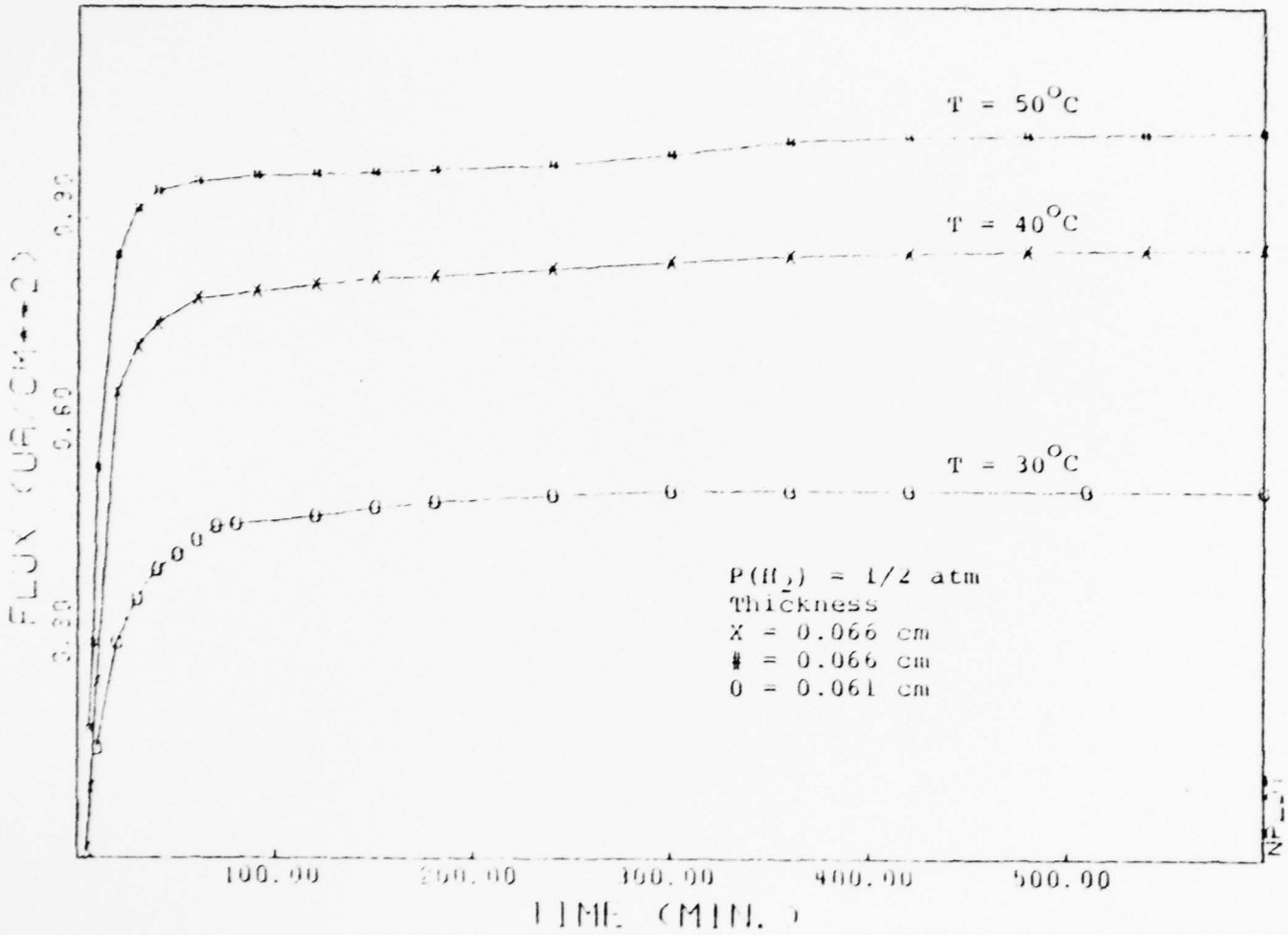

Figure 33: Absorption Transients at Various Temperatures.

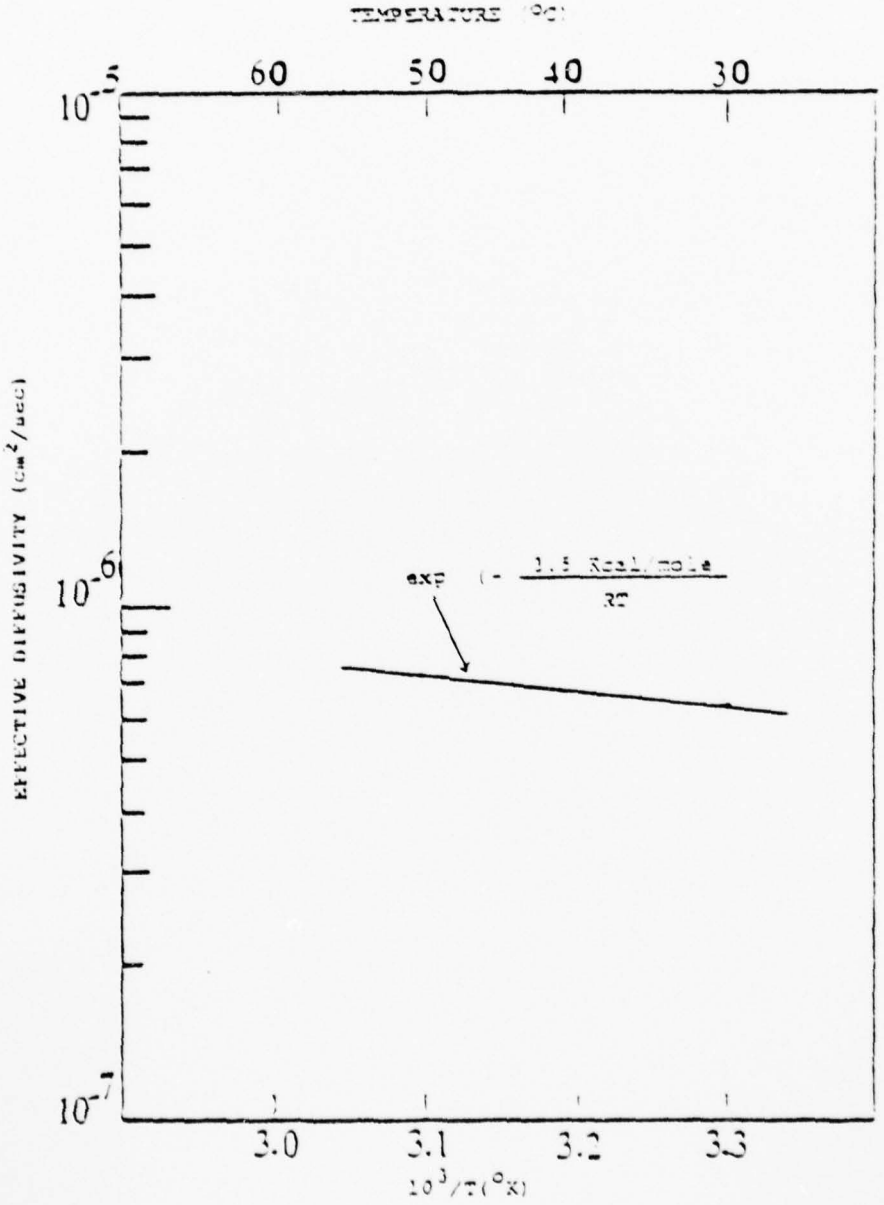

Figure 34: Effective Diffusivity as a Function of Reciprocal Temperature.

ture values taken from the data of Figure 5. This value is considerably lower than most of the low temperature values taken from the data of Figure 5.

The steady state flux was also observed as a function of temperature and the results are shown in Figure 35. A least squares fit of this data reveals an activation energy of permeation that agrees somewhat with the high temperature values of other researchers. Gonzalez[61] summarized and statistically analyzed most of the available permeation data and arrived at an activation energy of 8.5 $\pm$ 0.4 Kcal/mole within a 90% confidence level.

The disagreement between the two calculated activation energies deserves some consideration. A diffusivity activation energy of 1.9 Kcal/mole in the absence of trapping was predicted by Oriani[19]. The calculated value of 3.5 Kcal/mole, being considerably higher than Oriani's value, indicates that trapping may be occurring in this Ferrovac - E iron.

The agreement of calculated activation energy of permeation with the values of Gonzalez[61] is in dramatic contrast with the large deviation of calculated diffusivity activation energy with that of Oriani[19]. This situation can be rationalized if the difference in the two activation energies is considered. Measurement of the diffusivity involves the analysis of a structure sensitive property because of trapping[18]. Therefore disagreement or scatter among different researchers can be expected, due to

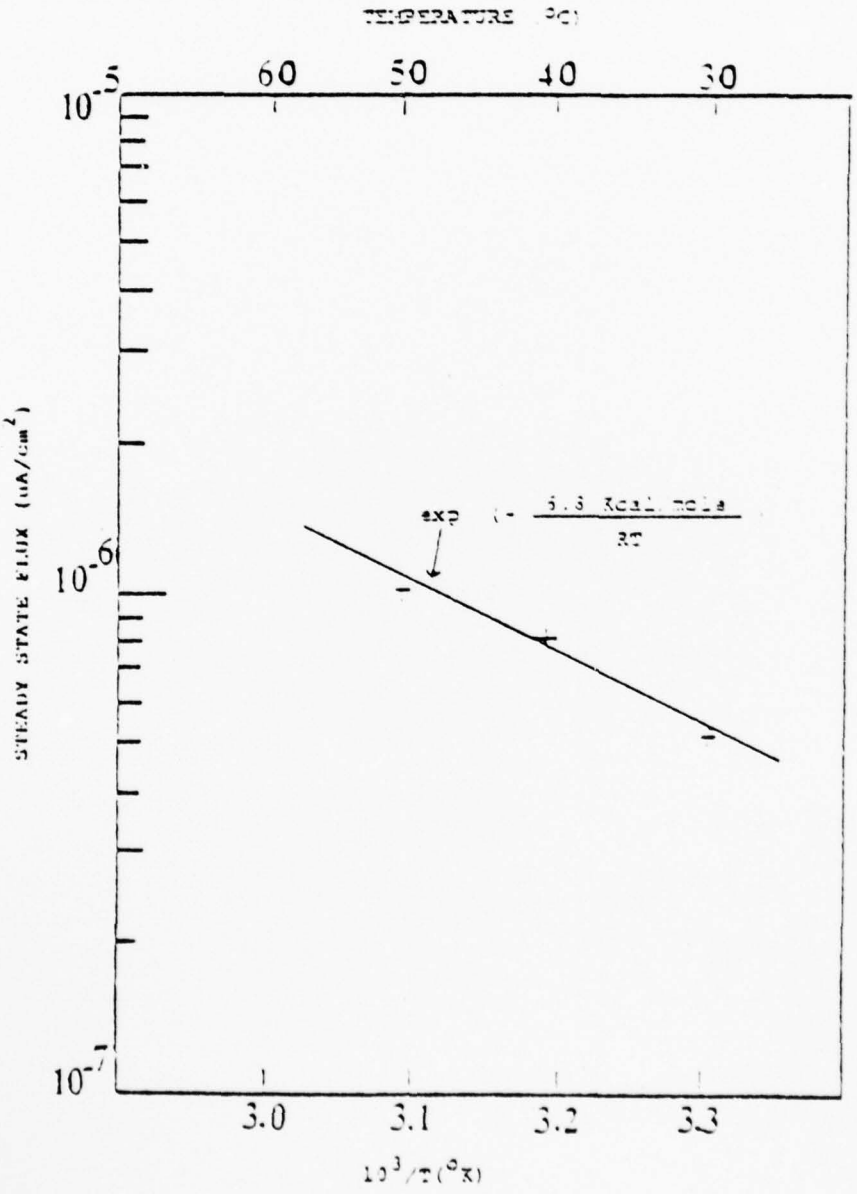

Figure 35: Steady State Flux as a Function of Reciprocal Temperature.

variance in metallic internal structures. But steady state permeation is not influenced by trapping because at steady state the lattice and trapped hydrogen are in equilibrium and lattice diffusion is the dominant process[18]. Therefore it is not surprising that reasonable agreement with literature values for permeation activation energy was obtained in this study.

4. Membrane Thickness Effects and Trapping

Figure 29 and Figure 32 showed the effect of membrane thickness on the calculated lattice and effective diffusivities. Other researchers have seen similar results of membrane thickness effects on effective diffusivity in permeability experiments where Ficks Laws are assumed to be valid[15, 18, 28, 62].

Quick[28] observed a thickness effect working with Ferrovac - E iron while using a gas phase charging technique at low temperatures. He observed no deviation from the linearity of the steady state flux versus inverse thickness plot; Fick's First Law was valid. At high temperatures no thickness effect was observed. He suggested that at high temperatures the thickness dependence on effective diffusivity gradually dampens out due to the thermalization of hydrogen from traps; when $D_{EFF} = D_L$ the thickness effect disappears. Shih[15] used zone refined annealed iron and observed the thickness effect at low temperatures while seeing no deviation from Fick's First Law. Radhakrishnan and Shreir[62] worked with Swedish iron at low temperatures found no thickness dependence on effective diffusivity in as received material. When they used material that had been annealed for two hours at 650^{o}C the thickness effect was detected. There was a substantial increase in effective diffusivity with increasing thickness. No deviation from Fick's First Law was observed.

In this study no deviation from Fick's First Law was observed. This can be seen from Figure 20, relating to Equation 6.

A possible explanation for the existence of the thickness effect is the surface area to volume ratio. When this ratio is large, as in the thinner samples, the surface effects will affect permeation more than when this ratio is small, as in the thicker samples[18].

If the values of lattice diffusivity, D_L, from Figure 27 are compared with the values of effective diffusivity, D_{EFF}, from Figure 28, it is seen that $D_L > D_{EFF}$ at the same hydrogen partial pressures. This can be attributed to the trapping that could be occurring in the iron. The lattice diffusivity is the diffusivity calculated if the only diffusion process occurring was lattice diffusion, in other words it does not take trapping into consideration. Effective diffusivity takes into consideration structure sensitive processes, such as trapping[18]. Therefore, it is expected that $D_L > D_{EFF}$. In this study it invariably is.

5. Pressure Effects on Permeation

Figure 36 is a plot of steady state flux versus the square root of hydrogen partial pressure at three different sample thicknesses. The relationship which exists between steady state flux and square root of hydrogen partial pressure is a linear one. This shows that Sievert's Law, Equation 2, holds true for this permeation study. Other investigations have reached similar conclusions[15,28].

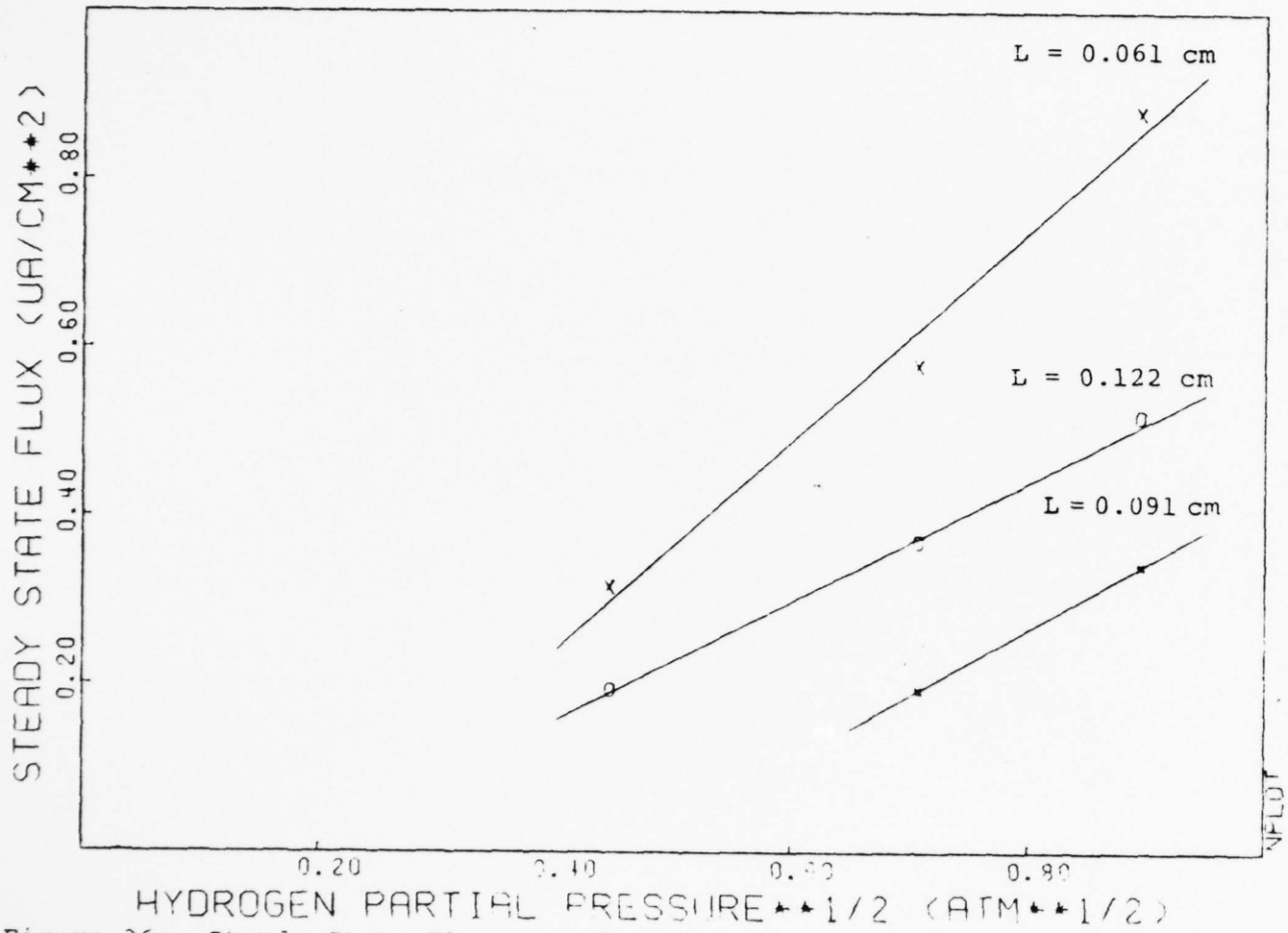

Figure 36: Steady State Flux as a Function of Hydrogen Partial Pressure

CHAPTER 4

SUMMARY AND NEW IDEAS

Gas phase hydrogen permeation curves have been obtained for Ferrovac - E iron. A steady state was always obtained, therefore the data analyses developed by McNabb and Foster [58], Boes and Zuchner[59] and McBreen et. al.[57] were used to calculate lattice and effective diffusivities. In this research the time to attain steady state was considerably longer than times reported elsewhere, the calculated effective diffusivities shown in Table 3 are slower than most of those reported by other laboratories and summarized in Table 1.

A membrane thickness effect on effective diffusivity was observed as shown in Figure 29. The effective diffusivity as calculated was observed to increase with increasing thickness of the specimen. The same sort of thickness effect has been reported by other researchers[15, 18, 28, 62]. A possible explanation for this thickness effect could be surface effects that impede hydrogen entry and permeation.

Comparing lattice diffusivity with effective diffusivity, Figures 29 and 32, it was observed that at the same hydrogen partial pressure lattice diffusivity is greater than effective diffusivity. The difference can be attributed to trapping that could be occurring in the iron[18]. Effective diffusivity takes internal structure effects such as trapping on diffusivity into account, while lattice diffusivity does not. Obviously effective diffusivity would

Table 3: Summary of Hydrogen Permeation Data Obtained in this Study.

Experimental Parameters					Measured Parameters			Calculated Results		
Sample Thickness L	Temperature T	Palladium Coating Thickness	Hydrogen Pressure $P(H_2)$	Original data appears in figure	Steady State Flux J_∞	$t_{0.83}$	Time Lag t_L	Effective Diffusivity D_{EFF}	Lattice Diffusivity D_L	Calculated or measured data are reported in figure
cm	^oC	^oA	atm		$\mu a/cm^2$	min	min	$cm^2/sec \times 10^{-7}$	$cm^2/sec \times 10^{-7}$	
0.064	30	2000	1/5	21	0.32	33	15	5.1	6.9	29,32
0.061	30	2000	1/2	22,25,26,33	0.52	25	12	6.2	8.6	29,32,34
0.061	30	2000	4/5	23	0.88	17	6.5	9.1	15.4	29,32
0.061	30	4000	1/2	26	.51	-	-	-	-	-
0.066	40	2000	1/2	33	.86	27	-	6.7	-	34
0.066	50	2000	1/2	33	1.00	25	-	7.2	-	34
0.122	30	2000	1/5	21	0.19	97	28	6.4	14.7	29,31,32
0.122	30	2000	1/2	22	0.36	80	17	7.7	20.6	29,32
0.122	30	2000	4/5	23	0.52	65	16.5	9.5	25.0	29,32
0.191	30	2000	1/2	22	0.17	130	28	11.6	36.1	29,32
0.191	30	2000	4/5	23	0.35	100	19	15.0	53.1	29,32
#0.064	30	Uncoated exit 2000 inlet	1/2	24	0.15	-	-	-	-	-

AD-A070 309 RHODE ISLAND UNIV KINGSTON DEPT OF OCEAN ENGINEERING F/G 11/6
HYDROGEN PERMEATION IN IRON AT LOW TEMPERATURES.(U)
MAR 79 M SURKEIN, R H HEIDERSBACH DAAG29-76-G-0311
UNCLASSIFIED TR-1 ARO-14057.3-MS NL

2 OF 2
AD
A070309

END
DATE
FILMED
7-79
DDC

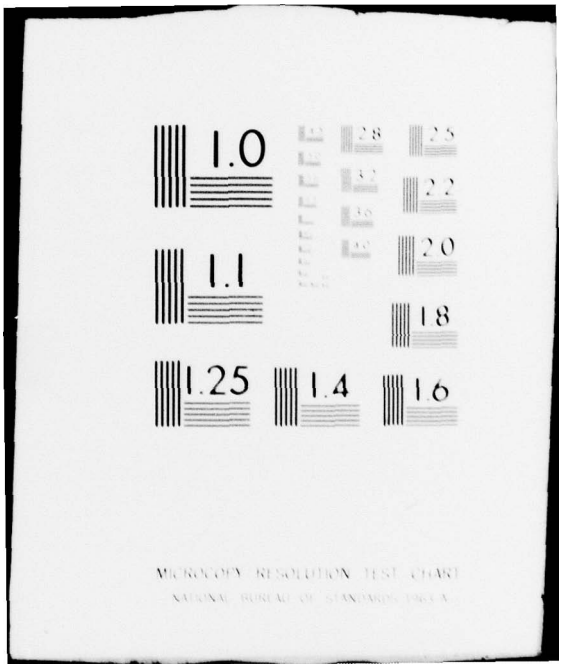
1.0
1.1
1.25
1.4
1.6
2.8
2.5
2.2
2.0
1.8
MICROCOPY RESOLUTION TEST CHART
NATIONAL BUREAU OF STANDARDS 1963 A

Table 3 (cont'd)

Experimental Parameters					Measured Parameters			Calculated Results		
Sample Thickness L	Temperature T	Palladium Coating Thickness	Hydrogen Pressure $P(H_2)$	Original data appears in figure	Steady State Flux J_∞	$t_{0.83}$	Time Lag t_L	Effective Diffusivity D_{EFF}	Lattice Diffusivity D_L	Calculated or measured data are reported in figure
cm	^oC	^oA	atm		$\mu a/cm^2$	min	min	$cm^2/sec \times 10^{-7}$	$cm^2/sec \times 10^{-7}$	
#0.060	30	Uncoated exit 2000 inlet	1/2	24,25	0.16	-	-	-	-	-
0.064	30	2000	1/5	16	0.33	2 - 9	16	5.8	7.1	-
0.061	30	2000	2/3	17,18,19	0.53 to 0.64	24 - 28	9 -11	5.5 - 6.5	9.4 -11.5	-
*0.061	30	2000	Electrochemical CD = 0.025 ma/cm^2	27	None	-	-	-	-	-

Diffusivities not calculated because not true bulk iron diffusivity

* Diffusivities not calculated because steady state not attained

be less than D_L.

Table 3 contains a summary of all permeation and diffustion data presented in this thesis. Comparing the effective diffusivity data in Table 1 with the data in Table 3, it is seen that the values calculated for effective diffusivity in this study are considerably slower than most of the values reported elsewhere. The slower calculated effective diffusivities can be explained by the longer times in this study to reach steady state than have been reported elsewhere. As previously mentioned in this thesis, long-term permeation curves have not appeared in the literature. If other researchers allowed their permeation curves to be extended, it is possible they would see the same result that has been seen in this study.

The experimental chamber as designed has the ability to reach temperatures in the range of 100°C. A higher temperature study seems to be the next step to investigate the so-called anomalous break in diffusivity data. To pursue this, a temperature chamber and possibly the experimental cell along with its apparatus need to be rebuilt to withstand the higher temperatures.

The gas flow system as built is designed to have an output pressure of 1 atm. High pressure permeation studies would complement high temperature experiments very nicely. A pressure chamber experimental cell would have to be built to pursue this sort of experimental testing.

An experimental set-up in which a sample could be stressed in a hydrogen environment while monitoring permeation flux could also be a direction to further this study. Experiments of this type have been reported by Bockris et. al.[27], Latanision et. al.[45] and others. Complicated factors would have to be taken into account such as the effects on the palladium coating or oxide film integrity.

CHAPTER 5

CONCLUSIONS

1. A thickness effect exists on the calculated effective diffusivity. As the experimental membrane thickness is increased, the calculated effective diffusivity also increases.
2. Steady state hydrogen permeation fluxes were obtained for all gas phase hydrogen permeation experiments performed in this research.
3. The times to reach steady state hydrogen permeation fluxes were substantially longer than times previously reported for low temperature hydrogen permeation studies on iron membranes.
4. Effective diffusivity rates for Ferrovac - E iron, calculated by the technique developed by McBreen, Nanis and Beck, were in the range of 5.1×10^{-7} cm^2/sec to 9.53×10^{-7} cm^2/sec at $30^{\circ}C$. These values are substantially slower than values reported elsewhere.
5. Lattice diffusivity rates for Ferrovac - E iron were calculated to be in the range of 6.9×10^{-7} cm^2/sec to 2.5×10^{-6} cm^2/sec at $30^{\circ}C$ by the technique of Foster and McNabb[58] as modified by Boes and Zuchner[59].
6. The calculated effective diffusivity increases as the partial pressure of hydrogen increases.
7. Inlet and exit sides of the experimental membrane must be electroplated with palladium to obtain true bulk

iron permeation data.

8. Calculated lattice diffusivity is shown to be greater than calculated effective diffusivity.
9. Fick's First Law of steady state flux varying linearly with inverse thickness was shown to be true.

BIBLIOGRAPHY

1. H. Deville, and L. Troost, Comptes Rendes, 57, 965-977, (referenced in C. Keuhler, "A Study of Hydrogen Permeation Through Metlas", Ph.D. Dissertation, Princeton University, 1974).

2. H.P. Van Leeuwen, Ph.D. Thesis, Delft Technological University, 1976.

3. D. Dull, Ph.D. Thesis, Univ. of California, Los Angeles, 1976.

4. R. McCright, Ph.D. Thesis, The Ohio State University, 1971.

5. H.K. Birnbaum, "An Overview of Hydrogen Failure Mechanisms", Naval Research Review, March 1977.

6. A.R. Troiano, F.W. Schaller and E.A. Steigerwald, Trans. Met. Soc. AIME, 218, 832, (1960).

7. C.F. Barth and E.A. Steigerwald, Met. Trans., 1, 3451, (1970).

8. W. Beck, E.J. Jankowsky and F.S. Williams, Corrosion, 27, 115, (1971).

9. I.M. Bernstein, "The Role of Hydrogen in the Embrittlement of Iron on Steel", ASTM Materials Science and Engineering, 6, 1, 1970.

10. H.H. Johnson, J.G. Morlet and A.R. Troiano, Trans. Met. Soc. AIME, 212, 528, (1958).

11. A.R. Troiano, Corrosion, 15, 207t, (1959).

12. C. Zapffe, J.I.S.I., 154, 123P, (1946).

13. M. Smialowski, Hydrogen in Steel, Addison-Wesley Publishing Co., Inc., Reading, Mass., (1962).

14. A.S. Tetelman and W.D. Robertson, Acta Metallurgica, 11, 415, (1963).

15. Hsiuan-Ming Shih, M.S. Thesis, Cornell Univ., (1975).

16. A. Sieverts, Z. Metallkunde, 21, 37, (1929).

17. E.W. Johnson and M.L. Hill, Trans. Met. Soc. AIME, 218, 1104, (1960).

18. A.J. Kumnick, Ph.D. Thesis, Cornell University, (1972).

19. R.A. Oriani, "Hydrogen in Metal", Proceedings of Symposium on Stress Corrosion, Columbus, Ohio, September 1967, p. 32.

20. C. Wert and C. Zener, Physics Review, 76, 1169, (1949), (referenced in Reference 17).

21. M.B. McNeil, J. of Applied Physics, 36, 7, (1965).

22. W. Geller and T.H. Sun, Arch. Eisenhuttenw, 21, 423, (1950), (referenced in Reference 15).

23. C. Sykes, H.H. Barton and C.C. Gregg, J.I.S.I., 156, 155, (1947).

24. T.M. Stross and F.C. Tompkins, J. Chem. Soc. 230, (1956).

25. Th. Heuman and D.Z. Primas, Naturforschj, 21A, 260, (1966), (referenced in Reference 15).

26. R.M. Barrer, Trans. of Faraday Society, 36, 1242, (1940).

27. W. Beck, J.O.M. Bockris, J. McBreen and L. Nanis, Proc. Roy. Soc., A290, 220 (1966).

28. N.R. Quick, Ph.D. Thesis, Cornell University, (1971).

29. H.G. Nelson and J.E. Stein, "Gas Phase Hydrogen Permeation Through α - Iron, 4130 Steel and 304 Stainless Steel From Less than 100°C to Near 600°C", NASA Report, TND-7265, (1972).

30. W.L. Bryan and B.F. Dodge, A.I. Ch.E. J., 9, 223, (1963).

31. M.L. Hill and E.W. Johnson, Trans. Met. Soc. AIME, 221, 622, (1961).

32. P.L. Chang and D.G. Bennett, J.I.S.I., 170, 205, (1952).

33. L. Darken and R.P. Smith, Corrosion 5, 60, (1949).

34. J. Bockris and P.K. Subramanyan, J. Elec. Chem. Soc., 118, 1114, (1971).

35. G. Hancock, Ph.D. Thesis, Cornell University, (1968).

36. R. Gibala, Trans. Met. Soc. AIME, 239, 1574, (1967).

37. M. Devanathan and Z. Stachurski, Proc. Royal Soc., 270A, 19, (1962).

38. T. Namboodhri and L. Nanis, Acta Metallurgica, 21, 633, (1973).

39. J. DeLuccia, Ph.D. Dissertation, Univ. of Penn.

40. J. McBreen and M. Genshaw, Proc. of the Conference on Fundamental Aspects of Stress Corrosion Cracking, 1967, Columbus, Ohio, NACE, 51, (1969).

41. J. Bockris, J. McBreen and L. Nanis, J. Elec. Chem. Soc., 112, 1025, (1965).

42. M. Devanathan, Z. Stachurski and W. Beck, J. Elec. Chem. Soc., 110, 886, (1963).

43. R. Heidersbach and J. Jones, "Optimization of the Electrochemical Hydrogen Permeation Technique", final report submitted to U.S. Army Research Office, Oct. 1976.

44. J. Jones, R. Heidersbach and M. Surkein, "Hydrogen Permeation of High Strength Steels", O.T.C. Paper 2801, May 1977.

45. R.M. Latanision, F.T.S. Lee and M. Kurkela, "Hydrogen Induced Intergranular Cracking of Nickel-Based Alloys", Technical Report No. 2 submitted to O.N.R., Oct. 1978.

46. R. Heidersbach, J. Jones and M. Surkein, Proc. of Second International Congress on Hydrogen in Metals, paper 4A3, Paris, France, June 1977.

47. N.D. Greene, Experimental Electrode Kinetics, Rensselar Polytechnique Institute, Troy, N.Y. (1965).

48. R. Heidersbach, Private Communication.

49. A.J. Kumnick and H.H. Johnson, Met. Trans., 5, 1199, (1974).

50. M. Pourbaix, Atlas of Electrochemical Equilibria, NACE, Houston, (1974).

51. R. Cusamano, M.S. Thesis, Univ. of Florida, (1971).

52. J.A. Barrie, J.D. Levine, A.S. Michaels and P. Wong, Trans. Faraday Soc., 59, 869, (1963).

53. G.S. Ansell, S.A. Koeffer and J.B. Hudson, Trans. Met. Soc. AIME, 245, 1735, (1969).

54. A.J. Kumnick and H.H. Johnson, Met. Trans., 6A, 1087, (1975).

55. S. Wach, A.P. Miodownik and J. Mackowiak, Corr. Science, 6, 271, (1966).

56. S. Wach, Br. Corr. J., 6, 114, (1971).

57. J. McBreen, L. Nanis and W. Beck, J. Elec. Chem. Soc., 113, 1218, (1966).

58. A. McNabb and P.K. Foster, Trans. Met. Soc. AIME, 227, 618, (1963).

59. N. Boes and H. Zuchner, J. of the Less-Common Metals, 49, 223, (1976).

60. R. Gurry and L Darken, Physical Chemistry of Metals, McGraw-Hill Book Company Inc., (1953).

61. O.D. Gonzalex, Trans. Met. Soc. AIME, 245, 607, (1969).

62. T.P. Radhadrishnan and L. Shreir, Electrochemica Acta, 12, 889, (1967).

63. J.O.M. Bockris and M. Devanathan, "Hydrogen Evolution: The Effect of Surface Concentration", Final report submitted to Office of Naval Research, March 1962.

64. W. Beck, J.O.M. Bockris, M.A. Genshaw and P.K. Subramanyan, Met. Trans., 2, 883, (1971).

65. J. Choi, Met. Trans., 1, 911, (1970).

66. M.G. Fontana, "Corrosion Cracking of Metallic Materials", report submitted to Air Force Materials Laboratory, Technical Report Number A.F.M.L. - 72-102, Part 1, 1972.